8-30-2019

Targeted Germanium Ion Irradiation of Aluminum Gallium Nitride/ Gallium Nitride High Electron Mobility Transistors

Melanie E. Mace

Targeted Germanium Ion Irradiation of Aluminum Gallium Nitride/Gallium Nitride High Electron Mobility Transistors

DISSERTATION

Melanie E. Mace, Major, USAF

AFIT-ENP-DS-19-S-025

DEPARTMENT OF THE AIR FORCE
AIR UNIVERSITY

AIR FORCE INSTITUTE OF TECHNOLOGY

Wright-Patterson Air Force Base, Ohio

The views expressed in this document are those of the author and do not reflect the official policy or position of the United States Air Force, the United States Department of Defense or the United States Government. This is an academic work and should not be used to imply or infer actual mission capability or limitations.

AFIT-ENP-DS-19-S-025

TARGETED GERMANIUM ION RADIATION OF ALUMINUM GALLIUM NITRIDE/GALLIUM NITRIDE HIGH ELECTRON MOBILITY TRANSISTORS

DISSERTATION

Presented to the Faculty

Department of Engineering Physics

Graduate School of Engineering and Management

Air Force Institute of Technology

Air University

Air Education and Training Command

in Partial Fulfillment of the Requirements for the

Degree of Doctor of Philosophy

Melanie E. Mace, B.S., M.S.

Major, USAF

September 2019

AFIT-ENP-DS-19-S-025

TARGETED GERMANIUM ION RADIATION OF ALUMINUM GALLIUM NITRIDE/GALLIUM NITRIDE HIGH ELECTRON MOBILITY TRANSISTORS

Melanie E. Mace, B.S., M.S.
Major, USAF

Committee Membership:

Dr. John W. McClory
Chair

Dr. James C. Petrosky
Member

Maj. Tod V. Laurvick, PhD
Member

Dr. Eric R. Heller
Member

ADEDEJI B. BADIRU, PhD
Dean, Graduate School of Engineering and Management

Abstract

Microscale beams of germanium ions were used to target different locations of aluminum gallium nitride/gallium nitride (AlGaN/GaN) high electron mobility transistors (HEMTs) to determine location dependent radiation effects. 1.7 MeV Ge ions were targeted at the gap between the gate and the drain to observe displacement damage effects while 47 MeV Ge ions were targeted at the gate to observe ionization damage effects. Electrical data was taken pre, during, and post irradiation. To separate transient from permanent degradation, the devices were characterized after a room temperature anneal for at least 30 days. Optical images were also analyzed pre and post irradiation. This is the first time localized dynamic irradiation testing has been used to compare AlGaN/GaN HEMT performance to the results of stress testing via in situ measurements of the gate and drain currents.

The 6 MV Tandem Accelerator at Sandia National Laboratories using the Micro-ONE system was used to induce displacement and ionization damage. Displacement damage was caused by 1.7 MeV Ge ions targeting the gate-drain gap of ten HEMTs in the off, on, and semi-on bias states where a fluence dependent delayed response between ion deposition and gate current degradation in the semi-on and on bias state was observed. The delayed response was also observed in the drain current degradation when biased in the semi-on state, while occurring immediately in the on state. Ionization damage was induced by 47 MeV Ge ions targeting the gate region in the semi-on bias state where gate current degradation occurred during the initial irradiation of the gate active region. Drain current degradation occurred in both the initial and subsequent irradiations. Pre and post irradiation output and transfer performance characteristics indicate drain current and transconductance degradation for

both experiments in all bias states. No threshold voltage shift was observed during the displacement damage experiment with 1.7 MeV Ge ions. During the ionization experiment, the threshold voltage increased after the initial irradiation with 2×10^{10} cm^{-2} 47 MeV Ge ions across the length of the gate. Subsequent irradiation over the same location and after a 60 day room temperature anneal did not change this threshold voltage shift and the decrease in the drain current and transconductance persisted, indicating permanent damage. The same performance characteristics changes have been associated with reliability stress testing causing similar effective damage in both the gate-drain gap and the gate regions. The observed degradation in device characteristics are consistent with the inverse piezoelectric effect in the displacement damage experiment and charge trapping in the gate region in the ionization experiment. These results show that radiation induced degradation can be captured by using a targeted ion beam in order to determine location dependent fluence limits, thereby informing both reliability and radiation hardness models.

For my two beautiful children. My son who asks me almost everyday, "when are you going to be finished with school and get a real job!" My daughter who still runs to me with joy whenever I enter the room.

Acknowledgements

I want to thank my advisor, Dr. McClory, for his ability to relate to my process and his willingness to go with it, for his ability to recognize the needs of my family and allowing me the time needed with them, and for pushing me when the push was necessary. I am thankful to Dr. Heller for his technical support and check-ins to help me continue forward. To Dr. Laurvick for his help and technical equipment assistance. To Dr. Petrosky for his support. To Gyorgy Vizkelethy, Edward Bielejec and the team at Sandia Ion Beam Laboratory for their help and support on this project. To Jeff Brown and Al Hilton for their help and assistance. I want to thank my Mom and Dad for always supporting me and helping when we needed it the most. Finally, I want to thank my husband and my two children for challenging me in new ways every day.

Melanie E. Mace

Table of Contents

Page

List of Figures

List of Tables

List of Abbreviations

Abbreviation		Page
Micro-ONE	Micrometer Resolution Optical, Nuclear and Electron Microscope	35
SMU	Source/Measure Unit	39
FINFET	Fin Field Effect Transistor	40
TEM	Transmission Electron Microscope	44

TARGETED GERMANIUM ION RADIATION OF ALUMINUM GALLIUM NITRIDE/GALLIUM NITRIDE HIGH ELECTRON MOBILITY TRANSISTORS

I. Introduction

1.1 Motivation

Industry requires semiconductor devices to be reliable throughout their intended lifetime. The military is undergoing major system redesign of strategic systems and advanced electronic components are important to the development. Radiation hardening is an important consideration during the planning phases of major military systems. Additionally, all technology used in major military systems must be reliable, there is no exception for radiation-hardened systems which require additional testing on top of reliability testing to be certified for use in military applications. Saving weight and space are preferred attributes in any solution for new military systems. Finding electronic solutions that allow for saving weight and space and are radiation hard and reliable has been an ongoing endeavor for the last fifty+ years, basically since the first transistors were created. As the space and weight requirements for semiconductors decrease, the electronics community has been working to advance new materials and structures that realize these desired attributes.

The increasing density and miniaturization of transistors in advanced integrated circuits results in increased power density and potential problems with heating and current leakage, leading to system degradation and eventual failure. Silicon-based power electronics have had a difficult time keeping up with the power density and energy efficiency requirements of the market. Device reliability requires an acceptably

low failure rate over some mission or lifetime, therefore, all potential failure mechanisms must be understood, mitigated, or fixed. Years of scientific research from a multitude of disciplines is normally required to fully understand and improve device design to maximize reliability in all operating environments and conditions. Devices based on silicon were the pathfinder for other device materials to follow. A vast amount of scientific and engineering advances have emerged over the past five decades throughout the entire electronics industry from manufacturing to device assembly and packaging for silicon based devices. Gallium arsenide (GaAs) based devices have been researched and improved over the past three decades and have become understood and reliable; they are the preferred transistor in certain functions.

An understanding of the capabilities and reliability of devices constructed from new materials require an understanding of the basic mechanisms of semiconductor design. New materials require investigation into finding the appropriate dopant, understanding the crystallography, determining the best materials to make Schottky and Ohmic contacts to optimize the device for specific applications, and determining the best structure for the required application. Within this process, failure mechanisms are analyzed and mitigated or fixed, if possible. New materials give rise to advantages for specific applications, particularly materials with narrow or wide band-gaps. Narrow band-gap materials are used in infrared detectors, optoelectronic and thermoelectric devices. Examples of narrow band-gap materials are germanium, mercury cadmium telluride, and indium arsenide. Wide band-gap (WBG) materials can be used at higher temperatures, power densities, voltages and frequencies. WBG materials used in power electronics have been made smaller and faster, thus reducing weight, volume and life-cycle costs while providing energy savings. Some promising wide band-gap materials include many elements paired with nitrogen termed "Nitride-based" such as aluminum nitride (AlN), gallium nitride (GaN), and alu-

minum gallium nitride (AlGaN). Other WBG materials include silicon carbide (SiC) and gallium oxide (Ga_2O_3). Some of these newer WBG materials are at the beginning phases of research; others, like GaN and AlGaN have moved toward the middle phase of development.

Smaller size and highly reliable radiation resistant device operation in high thermal, high frequency, high speed and high power environments are important for applications in space, nuclear and military fields. GaN high electron mobility transistors (HEMT) have advantages in some applications in these fields compared to silicon (Si) and/or GaAs devices, in particular GaAs HEMTS, allowing increased voltage and current to pass through the devices with greater efficiency and intrinsic radiation tolerance. However, GaN has been slow in meeting the reliability requirement because the failure mechanisms of GaN are more complicated than the dominant temperature-dependent failure mechanisms of Si and GaAs. GaN devices still lack qualification protocols for military space applications. Improved understanding of failure mechanisms within GaN technology is needed to reduce risks associated with these devices. Some of the military applications in development today would benefit from the improved technology, but it will only be used if the risks are reduced and the reliability is improved. This research aims to explore the use of targeted germanium (Ge) ion radiation at specific locations on an AlGaN/GaN HEMT device to observe performance characteristic changes that inform both the radiation and reliability communities.

1.1.1 GaN HEMTs and Reliability

GaN HEMT reliability is a topic of increasing interest particularly in power and radio frequency (RF) applications. Reliability predictions often use life-testing techniques based on the Arrhenius reaction rate equation which is temperature depen-

dent. Life-testing techniques used to qualify Si and GaAs devices, in particular GaAs HEMTs, for space application are not appropriate for GaN HEMTs because many of the failure mechanisms are not temperature dependent [1] [2] and multiple non-temperature dependent mechanisms may exist [3]. The wider band-gap allows a higher temperature operating regime causing other failure mechanisms to dominate. Multiple GaN HEMT failure mechanisms have been discovered resulting in a more complex reliability testing regime that is currently under development [3]. Understanding all of the failure mechanisms in GaN HEMTs is a first step to determining qualification requirements for space and military application. In 2018, the Aerospace Corporation released TOR-2018-00691 describing the "Guidelines for Space Qualification of GaN HEMT Technologies" by J. Scarpulla and C. Gee [3]. While guidelines are a good first step, there is a need for refined qualification protocol in areas including intrinsic reliability and the radiation environment.

1.1.2 GaN HEMTs and Radiation

GaN HEMTs have performed well in radiation environments due to the intrinsic radiation tolerance of the wider bandgap [4] compared to Si. The use of the Schottky diode gate technology instead of the oxide in Si MOSFETs also improves radiation tolerance because the oxide is known to be susceptible to total ionizing dose radiation effects. Usually radiation effects and electrical stress tests are accomplished separately, however, in recent years there has been work showing that when bias is applied while a part is irradiated, the bias state (on, off, semi-on) affects the relative change in threshold voltage and transconductance [5] [6]. After a combined space radiation and stress experiment, long term reliability effects were theorized, but the data was inconclusive prompting the need for more research in this area [7]. The environments resulting from a nuclear weapon detonation and from the natural space

background are different, but understanding the physics of failure can benefit analyses of device survivability in either case. Further research in how AlGaN/GaN HEMTs respond to applied bias and radiation is needed to understand the risks and limits when operating devices in a radiation environment when a bias is applied.

1.1.3 Qualification Challenges

In order for a semiconductor device to be qualified for space or military use, an understanding of the physics of failure is required. Tests are designed to accelerate the known failure mechanisms in order to predict and estimate end of life. All operating conditions and environments should be included in the qualification testing requirements to include intrinsic reliability and radiation effects. For GaN HEMTs, multiple failure mechanisms may exist and they may be different depending on operating conditions. Four direct-current stressing operating points, as described by where they fall on a current-voltage plot, have been identified: high power, high current with low voltage, high voltage with low current and off state. Two temperature tests are needed at each operating point to map the time to failure of multiple failure mechanisms appropriately [3]. Each stress operating point has been associated with different failure mechanisms.

Failure mechanisms have also been described as having location dependence under certain conditions, for example the drain edge of the gate [3]. Difficulty identifying failure mechanisms arise when multiple failure mechanisms are observed to cause similar changes to device performance characteristics. Therefore, stressing the device may cause multiple failure mechanisms to occur in each of the four regimes. Typically, radiation testing for reliability qualification is only included for devices that are required to operate in a radiation environment. For GaN, while radiation testing is accomplished for some devices marketed as space-qualified, a radiation standardized

testing protocol, as established for Si and GaAs devices, has not been defined for GaN HEMTs. Additionally, integrated reliability stress and radiation testing for devices that require radiation-hardening is currently not combined, rather separate tests are accomplished.

1.2 Radiation as a Tool

The Air Force was granted a patent application for using proton radiation as a tool for selective degradation and physics based device model test and calibration on October 25, 2018 [8]. The method involves using proton radiation to insert damage into specific locations of III-V compound semiconductors. A shield layer with high density is inserted over areas where damage is not desired and the proton energy is adjusted to reach locations where damage is desired, particularly in the channel. Results of electrical testing are compared pre and post irradiation for field-effect transistor devices [8]. Expanding on this methodology to include heavy-ions allows more types of damage to be created, such as higher energy displacement damage. Microbeam technology available at select accelerator facilities is able to target a specific location on a device which should allow the use of radiation as a controlled tool. In situ measurements should be able to be captured during microbeam irradiation as well and will be demonstrated during this research.

1.3 Link between Radiation and Electrical Stress Testing

Radiation interacts with atoms within the device structure causing ionization damage or displacement damage. During ionization damage, electron/hole pairs are created and the electrons are often carried away leaving the positive charge at or near the region of radiation interaction. This can cause a buildup of charge changing the electric potential creating the two dimensional electron gas (2DEG) and thereby

changing the performance of the device. During displacement damage, the crystal lattice is disrupted due to collisions between the lattice atom and the incident ion. Secondary damage from recoils can also cause additional damage in the device. Electrical stress testing can cause carriers to interact with defects by charging, dehydrogenation, or changing defect structures ultimately leading to device failure [6]. Different test conditions are designed to test for different failure mechanism phenomena, such as high-temperature operating bias tests for diffusion-related failure mechanisms in Si integrated circuits [9]. In Si MOSFETs, failure mechanisms such as electron/hole trapping, border and interface trap creation and hot carriers have a weak temperature dependence, therefore, an increased voltage rather than temperature is used to accelerate this failure mechanism during reliability testing [9]. These failure mechanisms can be created by ionizing radiation, high electric fields or hot carriers in the Si MOSFETs and each failure can result in increased degradation as buildup occurs [9]. In GaN, electric field induced gate leakage current and trapping and detrapping near the gate active region are known to cause failures under specific stress conditions. Electrical stress testing is designed by choosing different temperatures, voltages and annealing processes which accelerate specific failure mechanisms. Radiation has typically not been used to accelerate specific failure mechanisms, since radiation itself is a cause for failure. However, this research attempts to determine if radiation can be used to gain information that will aid in the understanding of failure mechanisms, particularly if defects created with radiation are the same as defects known to cause performance degradation without radiation.

A HEMT structure is similar to a MOSFET in that it is a field-effect transistor where the gate is controlled by applying a voltage bias. The interface is created by the combined piezoelectric and spontaneous polarization effect of the AlGaN and GaN. If the electric potential is changed by traps or lattice disruption, the 2DEG mobility and

carrier concentration will also be changed. Electrical stress testing has been shown to cause changes in performance characteristics such as threshold voltage shifts or decreases in transconductance [5] [11]. Performance characteristic changes caused by ionizing radiation or displacement damage in an AlGaN/GaN HEMT are similar to those observed during electrical stress testing [4]. A specific defect within the crystal lattice can be caused by multiple stress conditions to include proton irradiation, high electric field, and the semi-on state bias [11]. Thus, creating the defect using radiation could eventually establish correlations between radiation fluence under an applied bias and reliability lifetime testing allowing for an outside-the-box qualification protocol to be established.

1.4 Research Focus

This research used the 'radiation as a tool' concept from the patent application that was granted for proton radiation. However, instead of shielding, a microbeam attachment on an ion accelerator was used to target the radiation to specific locations in the device structure. This expands the methodology described in the patent and explores how heavy-ion damage rather than light-ion damage can be used as a tool for selective degradation. Targeting heavy-ion radiation into the gate-drain gap and the gate region causes damage to an AlGaN/GaN HEMT of a similar nature to that observed during electrical stress testing and provides information on how radiation targeting a particular location will degrade the device. To date, there are few experiments that have included radiation and applied bias or electrically stressed AlGaN/GaN HEMTs. The experiments that have been accomplished are limited to proton irradiation while the device is electrically stressed in situ or heavy-ion irradiation that stressed the device after irradiation occurred [5] [7]. Targeted heavy-ion, specifically the germanium (Ge) ion, radiation while stressed in a semi-on, on and off

state in the gate-drain gap and in the semi-on state in the gate region has not yet been explored and is the focus of this research.

1.5 Radiation through the Gate-Drain Gap

To determine if radiation can be used to understand failure mechanisms of AlGaN/GaN HEMTs, the region between the gate and the drain was explored by targeted 1.7 MeV Ge ion irradiation. This region of the device is known to have multiple failure mechanisms while under reliability stress testing [3] [12] [14] [15]. The devices were held at a constant bias in the off, on, and semi-on state during irradiation and the combined effect of the irradiation and bias is analyzed. Additionally, pre- and post-irradiation performance characteristics are measured and analyzed. Using heavy-ion irradiation to target a specific region of a AlGaN/GaN HEMT and measuring device electrical characteristics in situ is absent from the literature. Conducting a targeted in situ measurement provides insight into combined effects of heavy-ion irradiation and bias with a location focus. The results of this research may provide useful information for refining the qualification protocol of GaN technology for both the radiation and reliability communities.

1.6 Radiation through the Gate

The function of the gate region of a field-effect transistor semiconductor device is to provide the user control. The active depletion region is directly under the gate and the state of this region controls whether the device is on or off, based on the applied voltage on the gate. Targeting ions into the active region directly below the gate while obtaining an in situ measurement is absent from literature. A methodology to target this region of the gate was devised and accomplished. 47 MeV Ge ions were targeted through the active region of the gate of an AlGaN/GaN

HEMT while under a semi-on applied bias condition. In situ data and pre and post irradiation performance characteristics where measured and analyzed. The results of this research may help refine the qualification protocol of GaN technology for both the radiation and reliability communities.

1.7 Conferences and Publications

This research was selected as an oral presentation at two conferences, the Dayton-Cincinnati Aerospace Sciences Symposium (DCASS), Hardened Electronics and Radiation Technology Technical Interchange Meeting (HEART) and was an invited oral presentation at the Radiation Hardness Assurance (RHA) subcommittee session at the combined Joint Electron Device Engineering Council (JEDEC) and Society of Automotive Engineers (SAE) biannual meeting. An article has been submitted to the Journal of Radiation Effects Research and Engineering (JRERE) covering the content in Chapter 4. A second article is currently in process covering the content of Chapter 5.

1.7.1 Conference/Meeting Presentations

M. Mace, J. McClory, E. Heller. "Targeted Ion Radiation of AlGaN/GaN High Electron Mobility Transistors." 44th DCASS. Space Section II. ID: 44DCASS-044. March 5, 2019.

M. Mace, J. McClory, E. Heller, J. Petrosky, G. Vizkelethy. "Targeted Ion Radiation of AlGaN/GaN High Electron Mobility Transistors." HEART Emerging Technology Session. April 11, 2019.

M. Mace, J. McClory, E. Heller, J. Petrosky, G. Vizkelethy. "Targeted Ion Radiation of AlGaN/GaN High Electron Mobility Transistors." SAE CE11 RHA Users Subcommittee Meeting. May 15, 2019.

1.7.2 Publications

M. Mace, J. McClory, E. Heller, J. Petrosky, G. Vizkelethy. "Targeted Ion Radiation of AlGaN/GaN High Electron Mobility Transistors through the Gate-Drain Gap." Submitted to the *JRERE*.

M. Mace, J. McClory, E. Heller, J. Petrosky, G. Vizkelethy. "Targeted Ge Ion Radiation of AlGaN/GaN High Electron Mobility Transistors through the Gate." In process for submission to the *IEEE Transactions on Device and Materials Reliability*.

1.8 Document Overview

Chapter 2 presents background information of AlGaN/GaN HEMTs, radiation, stress, reliability and qualification. Chapter 3 presents the experimental methods used in both experiments described in the subsequent chapters. Chapter 4 discusses the results and analysis of targeting 1.7 MeV Ge ions into the gate-drain gap region of an AlGaN/GaN HEMT under different bias conditions. Chapter 5 discusses the results and analysis of targeting 47 MeV germanium ions into the gate of an AlGaN/GaN HEMT in the semi-on bias conditions. This document concludes in Chapter 6 with a summary and proposals for future work.

II. Background

2.1 GaN HEMT Reliability

An AlGaN/GaN HEMT is a Modulation Doped Field Effect Transistor (MODFET); it has also been called a Heterojunction Field Effect Transistor (HFET) in literature. A MODFET relies on the creation of a 2DEG conduction channel. The 2DEG is a quantum well which limits scattering creating a higher mobility device. The original MODFET was created using doping profiles in AlGaAs/GaAs HEMTs. In an AlGaN/GaN HEMT the conduction band-gap of the AlGaN/GaN heterostructure forms a quantum well without doping. The heterostructure's band-gap is influenced by polarization effects which are caused by spontaneous III-N atomic polarity creating strong built-in fields increasing the number of polarity-bound charge carriers. Additionally, a piezoelectric effect due to the crystal strain at the interface of the AlGaN and GaN contributes to the polarization field. The energy bands bend in such a way that a potential well is formed that dips below the Fermi level of the heterojunction at the interface between the AlGaN and GaN; thus trapping the electrons in a 2DEG. Crystal strain modifies the electric field properties shifting the quantum well structure of the 2DEG and ultimately changing the key performance characteristics of the device.

GaN is a III-V material that is stable in the wurtzite crystal structure at room temperature and atmospheric pressure. The III-V structure causes a slightly more ionic bonding than in a column IV covalent dominant structure. The in-plane lattice constant is 0.3189 nm and the axial lattice constant is 0.5185 nm [16]. GaN can also form in a zinc blende cubic structure under different pressure and temperature conditions with a lattice constant of 0.4520 nm [16]. GaN is a direct band gap material which means that the conduction band valley and valence band peak line

up exactly at the Γ point in the wurtzite structure. The conduction band has two additional valleys and the valence band has a heavy hole, a light hole, and a split off band in the wurtzite structure as shown in Figure 1 [16]. The energy needed to

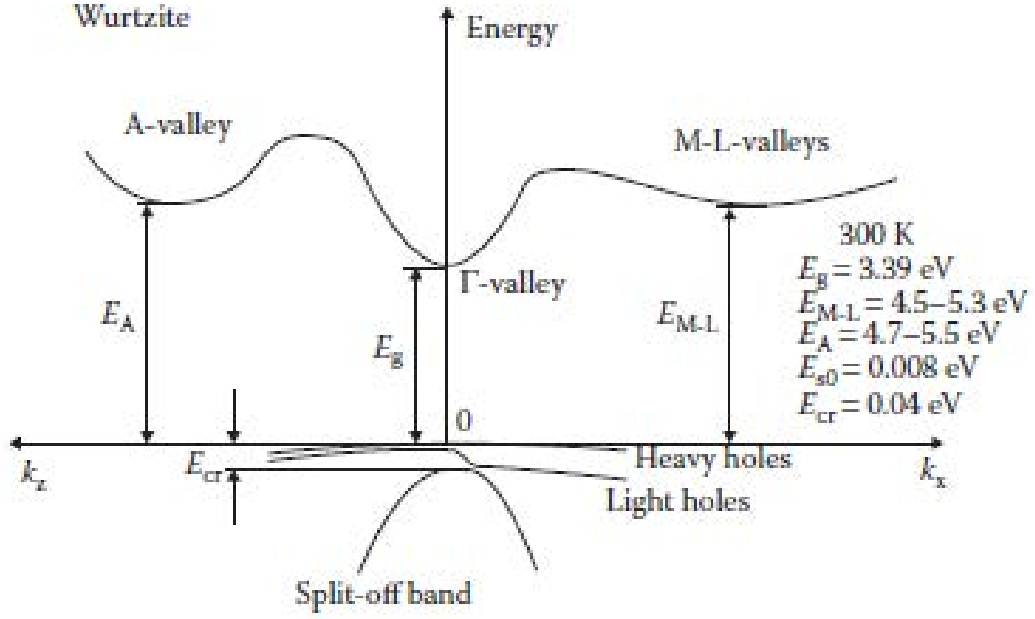

Figure 1. GaN wurtzite band structure. Reproduced with permission from [16].

excite an electron from the valence band to the conduction band is much greater due to the wide band-gap, establishing a larger energy tolerance to changes in the GaN's electrical characteristics under perturbing condition such as increased thermal energy or radiation absorption. High power environments are more accessible to a wide band-gap and for the HEMT structure.

The direction of crystal polarity depends on the atom making up the top face (gallium or nitrogen) during the growth process. Since the GaN is slightly ionic, there is already a dipole moment between the positive nucleus and the negative electrons within the structure. The existing dipole moment induces a spontaneous polarization across the polar axes. With an applied stress, the dipole moments will become

stronger or weaker depending on the separation distance of the centers of positive and negative charge. Across the crystal, this effect becomes significant and is called piezoelectric polarization. When two materials of different crystal lattice spacing are grown on top of each other, there is a strain placed on the interface. The crystal with the larger spacing will experience a compressive (tensile) strain by being forced to grow with a tighter atomic spacing than normal. When the atoms are strained, the electrons are offset slightly from their normal position relative to the nuclei creating an electric field. Since the lattice constants do not match exactly at the interface between AlGaN and GaN, a strain induced piezoelectric field is created along the c-axis of the AlGaN/GaN structure and is dependent on the crystal polarity as described in Figure 2 [16]. There are different conditions for polarization depending on whether the AlGaN or GaN is strained or relaxed and how the two types of polarization combine. The spontaneous and piezoelectric polarization add to create a net charge which creates an electric field that becomes larger during the growth of the AlGaN layer. Surface electrons are swept into the electric field induced well at the interface which adds carrier concentration to the 2DEG. The piezoelectric effect can be weakened by a concept called strain relaxation if the thickness of the buffer layer is large or the percentage of aluminum is large; for AlGaN/GaN as the AlGaN thickness increases the 2DEG density increases and then saturates [16]. A passivation layer on the surface is often used to moderate changes in strain caused by surface states formed when the surface electrons get swept to the 2DEG leaving behind the positive ions (acceptor-like AlGaN surface states) which can cause a virtual gate effect or trap electrons reducing the number of carriers in the 2DEG [16]. This passivation layer is often silicon nitride, and is the material used on the devices for this research.

An electrostatic analysis of an AlGaN/GaN heterostructure can be accomplished to determine the number of carriers in the 2DEG. Figure 3 shows the heterojunction

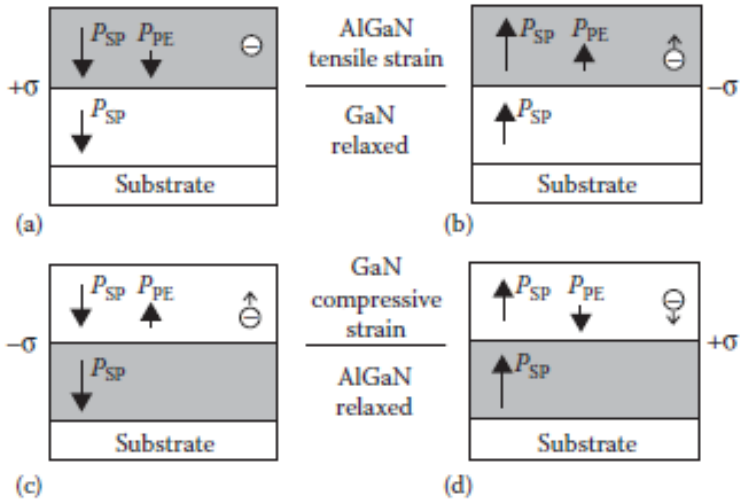

Figure 2. AlGaN/GaN polarization from spontaneous and piezoelectric effects dependent on polarity of crystal. (a) Ga-face interface, the spontaneous and piezoelectric polarization of the AlGaN combine. (b) N-face interface, the spontaneous and piezoelectric polarization of the AlGaN combine. (c) N-face interface, the spontaneous and piezoelectric polarization of the GaN oppose each other. (d) Ga-face interface, the spontaneous and piezoelectric polarization of the GaN oppose each other. Reproduced with permission from [16] and Reprinted from O. Ambacher, et al. Journal of Applied Physics. 85(6). 3222. 1999, with the permission of AIP Publishing [17].

band gap of the AlGaN/GaN interface (top), the carrier density associated with the electric field (middle) and the spatial distribution of the AlGaN and GaN (bottom) [16].

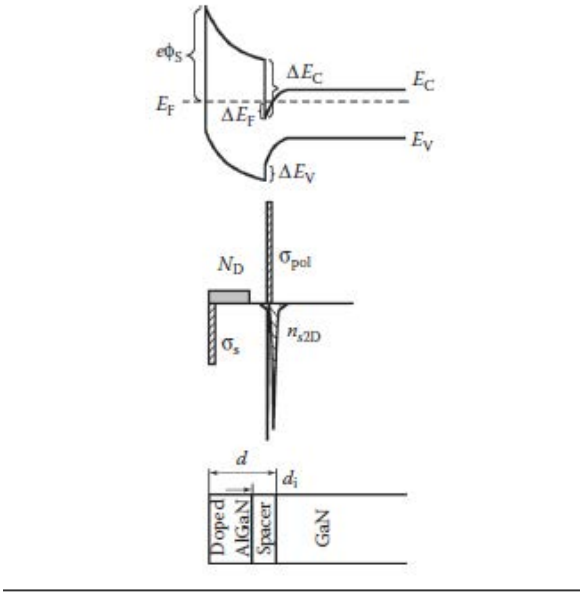

Figure 3. AlGaN/GaN energy band structure and charge distribution. Reproduced with permission from [16].

2.1.1 Stress Testing

Understanding how stress is created under varying operating conditions informs models and allows device designers to anticipate reactions in differing environments. Stress affects the reliability of a device if it fails during normal operation in a way that is not anticipated. Stress can be created in a number of ways, for example in silicon devices, high temperature environments are the ultimate stress affecting reliability. As such, the main lifetime reliability stress test in silicon is temperature based. For GaN, Christiansen showed that temperature was not always the dominant lifetime reliability failure mechanism that should be considered [1]. Instead, multiple failure mechanism have been identified; it is difficult to determine the cause based

on performance characterization but recent work has been accomplished to develop a methodology [19][20].

Stress conditions can include increased temperature, DC voltage, or RF bias, as well as radiation and mechanical stress. Each has a different effect on the device reliability and over-stressing conditions can cause device breakdown. Degradation can also occur and is caused by stress conditions to the point that a device will not operate within the necessary operational parameters. Each stress condition listed above causes failure mechanisms within a device. Understanding the failure mechanisms leads to an improved understanding of reliability leading to the design of mitigation methods that can be employed once the mechanism is known and understood. For AlGaN/GaN HEMTs the known failure mechanisms include thermal, hot electrons, electron trapping, and electric field induced gate leakage current.

Current methods for determining lifetime reliability for transistors involve temperature and electrical stressing of devices for up to 1000 hrs to replicate the lifetime conditions of what the device would experience in a more realistic time frame. This works well for silicon, however with GaN, there are failure mechanisms that dominate at different stress conditions that are not well understood.

GaN HEMTs have not yet had a standardized process developed for space qualification, DC stressing alone may not be sufficient due to multiple failure mechanisms and higher temperature, voltages, and power densities than previous device materials [3]. Signature parameters have been correlated with mechanisms observed which dominate different zones in the drain I-V plane [19]. Changes to maximum drain current appear to be linked to surface pitting adjacent to the gate for the high voltage and low current zone [3][19]. Hot electron generation of fixed charge embedded within the layers and passivation distributed between the gate and the drain causing local pinch-off, which reduces current mostly in the saturation region, is a signature pa-

rameter of reduced peak transconductance and occurs in the high power state [3][19]. The high voltage off state is linked to electron trap generation and population changes which affect the gate depletion region; a signature parameter of trap generation in this state is a change to threshold voltage [3][19]. New guidelines derived for qualification test campaigns require two temperature measurements at each of the four states. The fourth state is the high current, low voltage state associated with thermal failure mechanisms [3][19].

The physics of failure mechanisms of GaN are complex and when grown as an AlGaN/GaN HEMT, the complexity increases. AlGaN/GaN HEMTs are not grown on a native substrate. This increases its susceptibility to dislocations and creates a complex region near the channel [14]. The drain edge of the gate has many observed findings involving mass-movement which causes performance degradation such as point defects, intermixing, pitting and cracking. Additional defects include defect percolation, surface charging, dislocation and diffusion [14]. Improved reliability of these devices can occur by finding solutions to mitigate these problems. Therefore, fully understanding the physics of these failure mechanism is important.

2.1.2 AlGaN/GaN HEMT Failure Mechanisms

Reliability issues of GaN-based HEMTs are tied to current collapse and performance characteristics changing outside of the operational margin limits. The failure mechanisms of interest for the last decade for the AlGaN/GaN HEMT include hot electron, electron trapping, and electric-field induced gate leakage. Isolating the failure mechanism and identifying the performance characteristic change has been difficult. For electric field induced gate leakage, the failure mechanism can involve an inverse piezoelectric effect at the gate edge, electrochemical dissolution, or extended erosion and cracks, and there may be a time dependence to the mechanisms and the

performance characteristics that reduced drain current [19][20][21]. Permanent and recoverable trapping and detrapping effects near the gate affecting the gate depletion region results in a threshold voltage shift [19], [20]. Hot electrons that cause fixed charge to distribute between the gate and drain or embed within the layers has been linked to reduced transconductance [19] [20]. Over the past 10 years, researchers have been able to isolate the stress regimes that cause the specific failure mechanisms observed in DC stress testing. The three AlGaN/GaN HEMT failure mechanisms listed below have been isolated by specific stress testing conditions [16][19][20][21]:

1. Hot Electrons
2. Electron Trapping
3. Electric Field Induced Gate Leakage Current

This research uses radiation as a tool to cause similar performance degradation as observed during stress testing for failure mechanism 2 and 3.

2.1.2.1 Electric Field Induced Gate Leakage Current

Gate leakage current can be increased due to a high electric field at the drain-side of the gate edge. This is caused by a number of failure modes. First, the piezoelectric effect can be counteracted by the high electric field which may reduce the actual quantum well depth, changing the 2DEG. Additionally, the inverse piezoelectric effect can create new electron traps from nucleation defects or lattice relaxation from the AlGaN/GaN barrier expansion [16][21]. If the inverse piezoelectric effect causes strain that is too large for the crystal lattice to absorb, cracks and extended erosion has been observed which causes irreversible damage [21]. Second, the gate can degrade over time from the high electric field creating traps that form a conductive percolative path between the gate and channel [21]. Third, pits and grooves from electrochemical

dissolution of GaN can be formed when oxygen and/or water vapor combine with Ga or Al forming oxides that contribute to surface oxidation and interface oxidation [21]. A permanent decrease of drain current is attributed to pits, extended erosion and cracks across the epitaxial layers [21].

Gate current leakage can occur in GaN due to high reverse bias which causes an inverse piezoelectric effect to occur that generates defects because of the intrinsic piezoelectric properties of GaN and AlGaN [22]. This could be caused by the interface of AlGaN/GaN to undergo inelastic strain caused by the high bias [22]. In 2012, there were multiple theories surrounding the cause of the inverse piezoelectric effect, from electric field induced mechanical stress resulting in the relaxation of the AlGaN layer to a contrasting theory that higher temperatures cause thermal stress/strain mitigating the natural piezoelectric stress [22].

When an electric field is large in a piezoelectric material, it can counteract the electric field ultimately reducing the channel depth. It can also be strong enough to actually crack the material which then strains the structures in a different way. However, it is not only an inverse piezoelectric effect that can occur. Gate leakage has also been noted, so not only is the current reduced by a change in the depth of the well, but the number of carriers in that well also changes from gate leakage due to a high electric field.

The strong electric field in the AlGaN/GaN barrier leads to lattice relaxation and creates new lattice defects which act as electron traps. This causes an additional gate leakage current because the number of carriers in the 2DEG is affected by the number that are caught in the electron traps. Transmission electron microscopes have been used to see tiny cracks that have formed at the gate edge on the drain side after stress due to strain from the inverse piezoelectric effect [16].

To see the effects of increased gate leakage current from a high electric field, step-stress tests have been found to be the best method to verify the presence of this failure mechanism [21]. The step-stress test is performed by having V_S and V_D = 0 V, the V_G decreasing in steps of -2 V to -5 V to a large negative bias while holding each bias for a duration of 2 minutes. In Figure 4, the step-stress gate voltage decreased

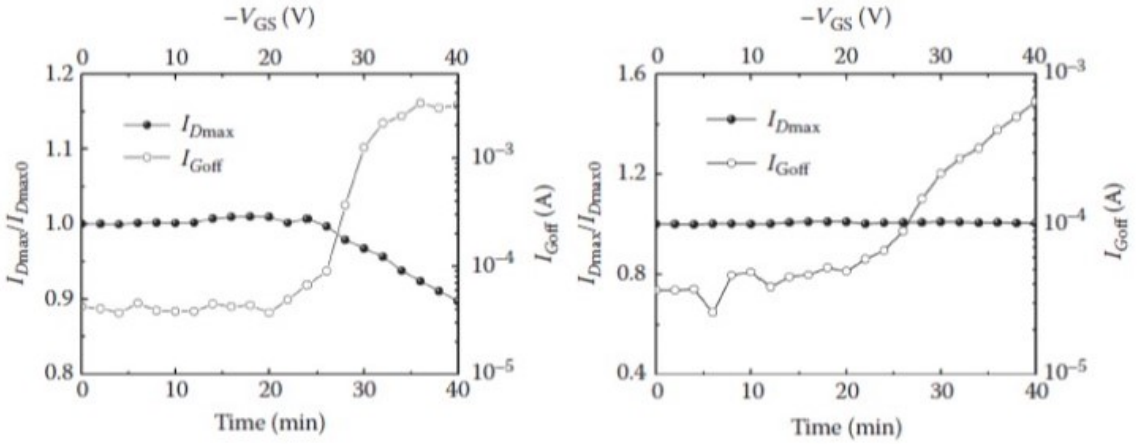

Figure 4. Variation of I_{Dmax} and I_{Goff} under stress. Note that V_{GS} increases in the negative direction with longer stress time. (Left) without a GaN cap layer (Right) with a GaN cap layer. Reproduced with permission from [16].

from 0 V to -40 V in steps of -2 V while holding each bias for a 2 min duration at each step. IV characteristics were taken at each step, $I_{dmax} = I_d$ at V_{ds}=5 V, V_{gs}= 2 V and $I_{Goff} = I_g$ at V_{ds}=0 V, V_{gs}= -10 V [16].

Figure 5 shows results over time of a similar stress test as Figure 4 where V_S=V_D=0 V and V_G decreases from -10 to -80 V with -5V/step, step duration 2 min [21]. Figure 6 shows that the time to breakdown depends on the electric field.

2.1.2.2 Electron Trapping

Threshold voltage shift and degradation in transconductance are attributed to trapping and detrapping effects [21]. Electron trapping near the gate causes changes to the depletion region [20]. The zone associated with electron trapping has been

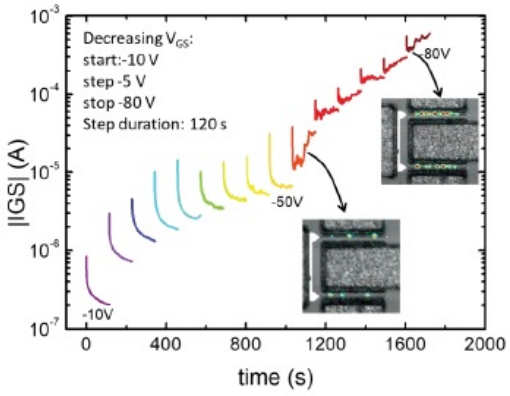

Figure 5. Variation of gate current during a step-stess experiment carried out with V_S=V_D=0V and V_G decreasing from -10V to -80V with -5V/step, step duration 2 min. The two insets report the false color EL maps measured after two different stages of the stress experiment. ©[2013] IEEE [23].

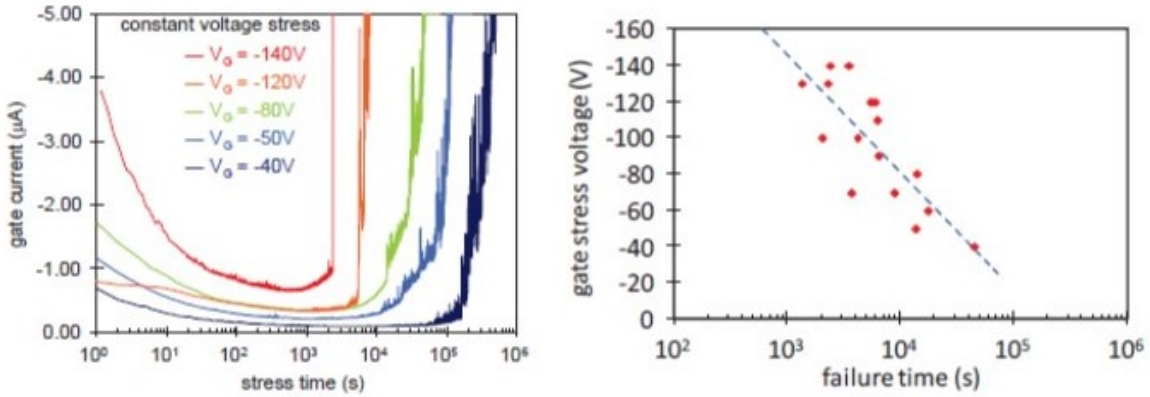

Figure 6. Left: I_G versus time to breakdown experiments demonstrating the dependence of the time to gate leakage breakdown on the applied reverse voltage for AlGaN/GaN HEMTs. Right: Power-law relating failure time to gate stress voltage. ©[2013] IEEE [23].

in the off state, with a high drain voltage [19]. Recent research using low-frequency noise measurements to identify defects responsible for stress-induced degradation has also been conducted [5][11]. Positive threshold voltage shifts can be observed either in the on state, due to the creation of acceptor-like traps in the channel, or the off state, when there is a high drain voltage applied due to creation of acceptor-like traps in the gate-drain gap region also near the channel [11]. Because the traps are near the channel, mobility is reduced causing a reduction in transconductance as well. It was found that the off state threshold voltage shift was dependent on the drain voltage as to whether the shift would be positive or negative indicating that multiple types of defects are responsible for threshold voltage shifts and processing differences affect the shifts [11].

2.2 GaN Radiation Performance

GaN HEMT technology has typically performed very well in radiation environments. This success has been attributed to the wider band-gap and the increased bond strength of the crystal [4]. Within the past few years increased research in GaN HEMTs crosses into both the reliability and radiation communities. Vanderbilt University's Institute for Space and Defense Electronics has performed work coupling radiation with different performance states noting that applied bias makes a difference in performance characteristics under radiation conditions, particularly threshold voltage and transconductance [5] [6]. Long term reliability is also of interest in general and when coupled with radiation. Understanding how radiation affects long-term reliability in GaN HEMT devices is not currently well understood and research in this area is emerging [7]. While this may be new work for GaN, similar failure mechanisms have been observed in other device material systems [9]. In Si MOSFETs, failure mechanisms of electron/hole trapping is known to lead to border traps and

ultimately lead to interface traps [9]. This process is known to be caused by either a high electric field, hot carriers, or ionizing radiation [9]. These traps lead to threshold voltage shifts and/or mobility reduction and are known to have a weak temperature dependence [9]. The trapping failure mechanism accelerated tests for MOSFETs were based on increased voltage rather than temperature [9].

There are two types of irradiation damage mechanisms: ionization and displacement damage. Ionization is the creation of electron/hole pairs by charged particles interacting with the electrons in the target material. Displacement damage is the movement of the target atom away from the normal lattice position to another position in the lattice creating an interstitial/vacancy (Frenkel) pair. This section will discuss the physics and impact associated with radiation interactions.

For protons, which are charged particles, ionization is the main cause of damage which occurs through the electrostatic force interactions. Displacement damage can also occur through nuclear interactions. For protons scattering in GaN, there is a threshold energy of 440 eV (19.5 eV displacement energy threshold, E_d [24]) that is required to remove (knock) the atom from the lattice site. Higher energy protons can also cause significant degradation due to displacement damage. The "hard sphere" collision model can be used to determine the number of displaced atoms, N_d, produced by primary knock-on atoms (PKA) as shown in Equation 2.1 [25]. Therefore, a collision between a GaN atom and a $E = 4$ MeV proton can produce up to 1.02x10^5 Frenkel pairs. However, 4 MeV is enough energy to cause complicated damage regions (cascades or clusters) [25]. Monte Carlo calculations such as Stopping and Range of Ions in Matter (SRIM) and the associated transport code (TRIM) can be used for this type of analysis [33].

$$N_d = \frac{E}{2E_d} \tag{2.1}$$

The overarching radiation effects caused by ionization or displacement damage are carrier lifetime damage, carrier removal and mobility degradation. Lifetime damage affects the minority carrier lifetime and therefore the diffusion length due to an increase in recombination with the minority carrier [25]. Mobility degradation is caused by increased scattering from increased impurities within the bandgap [25]. Because the AlGaN/GaN HEMT is a majority carrier device, and relies on a 2DEG, minority carrier lifetime and mobility changes should not be a dominate radiation effects. However, carrier removal can affect the Fermi level of the device. The number of defect centers increases with an increase in the number of Frenkel pairs. This increase in Frenkel pairs can change the Fermi level because it can change the carrier concentration in the valence and conduction bands. These defect centers can have energy levels within the bandgap, thereby reducing the number of carriers in the valence band and conduction bands resulting in reduced carrier availability for current. The carrier removal process is a dominant effect in heterojunctions such as AlGaN/GaN HEMTs; carriers are trapped in locations other than the 2DEG which reduces the carrier concentration inside the 2DEG channel of the HEMT. Effects specific to a heterojunction structure include increased tunneling across the thin heterostructure barrier, changes in sheet charge that affect the carrier density within the 2DEG, and changes in the energy level traps within the quantum well structures [25]. However, as the crystal lattice is deformed near and around the interface, mobility can be affected due to scattering in addition to loss of carrier concentration.

For silicon and gallium arsenide the current methodology is to use non-ionizing energy loss (NIEL) to describe the damage from displacement effects. For protons

less than 10 MeV, the hard sphere collisions are dominant and NIEL calculations and experimental results agree satisfactorily [25]. Changing results from one experiment to a standard 1 MeV NIEL equivalent allows different devices to be compared to determine their relative radiation hardness susceptibility.

Annealing is the process where the crystalline structure reorders in a way that may recover electrical performance characteristic degradation caused by stress or irradiation. Annealing can occur over time while a device is at room temperature. Annealing can also occur by increasing the temperature of electrical current of the device. Annealing can make radiation damage worsen or improve device characteristics depending on the type of damage created. Permanent damage will not recover during annealing. Typically, reliability testing and qualification protocols include annealing in the instructions.

Ions can interact with nuclei and electrons of a target material which cause the ions to lose energy through nuclear and electronic stopping mechanisms. Electronic stopping power, an inelastic process, dominates at lower atomic number and higher ion energies creating excitation of bound electrons and thermal vibrations as well as ion electron cloud excitations [4]. Conversely, nuclear stopping, an elastic process, dominates at higher atomic number and lower velocities which creates deep-level compensating defects [4]. Fast ions tend to travel too quickly though the material to interact with the nucleus and therefore the capture cross section is lower reducing the displacement damage observed.

The linear stopping power, S, (also called specific energy loss or the rate of energy loss) is defined as the differential energy loss (dE) per differential path length (dx) of a charged particle within the material and is described by the Bethe formula as shown in Equation 2.2 which is valid for velocities of primary particles larger than orbital electron velocities [26].

$$S = -\frac{dE}{dx} = \frac{4\pi e^4 z^2}{m_0 v^2} NZ[ln\frac{2m_0 v^2}{I} - ln(1 - \frac{v^2}{c^2}) - \frac{v^2}{c^2}] \tag{2.2}$$

In equation 2.2, v = velocity of primary particle, ze = charge of primary particle, N = number density of absorber atom, Z = atomic number of absorber atom, m_0 = electron rest mass, e = electronic charge, I = average excitation and ionization potential of the absorber, and c = speed of light.

For GaN, both the nuclear stopping power and the electronic stopping power can be calculated according to Equations 2.3 and 2.4 [4].

$$S_N(E_0) = 8.462 \times 10^{-15} Z_1 Z_2 M_1 \frac{S_N(\epsilon)}{(M_1 + M_2)(Z_1^{0.23} + Z_2^{0.23})} \tag{2.3}$$

where Z_1 is the atomic number of the ion, Z_2 is the average atomic number of Ga and N, M_1 is the mass of the ion and M_2 is the average mass of the Ga and N atoms [4].

$$S_{eb} = \frac{8\pi Z_1^2 e^4}{I_0 \epsilon_b} ln(\epsilon_b + 1 + \frac{5}{\epsilon_b}) \tag{2.4}$$

where

$$\epsilon_b = \frac{4E(\frac{me}{M_1 m_0})}{Z_2 I_0} \tag{2.5}$$

and m_0 is the atomic mass unit, M_0 is the relative atomic mass of the ion and I_0 is the Block constant in units of electron volts (eV) [4].

The Bragg curve describes the specific energy loss (stopping power) of a charged particle along a track across the distance of penetration. There is usually a low energy loss at the beginning with the charged particle losing most of its energy at a specific location within the material.

2.3 Performance of Irradiated GaN Devices

2.3.1 Damage from Light-Ions and Heavy-Ions

Reduction in carrier concentration and mobility due to trapping are the main radiation induced defects causing an observed decrease in saturation current, transconductance and threshold voltage shifts [4]. Light-ions, like protons, are dominated by electronic stopping where the nuclear stopping dominates the heavy-ion interaction leading to considerable lattice damage [4]. Single event effects have been studied by using heavy-ions such as He, C, Fe, Br, Xe, Kr, Ne, Ar [4]. Proton work has found that the rate of change for threshold voltage, mobility and transconductance decreased with increasing proton energy or fluence correlating to the energy deposited into the AlGaN barrier and the 2DEG [4]. Modeling conducted by E. Patrick et al. identi-

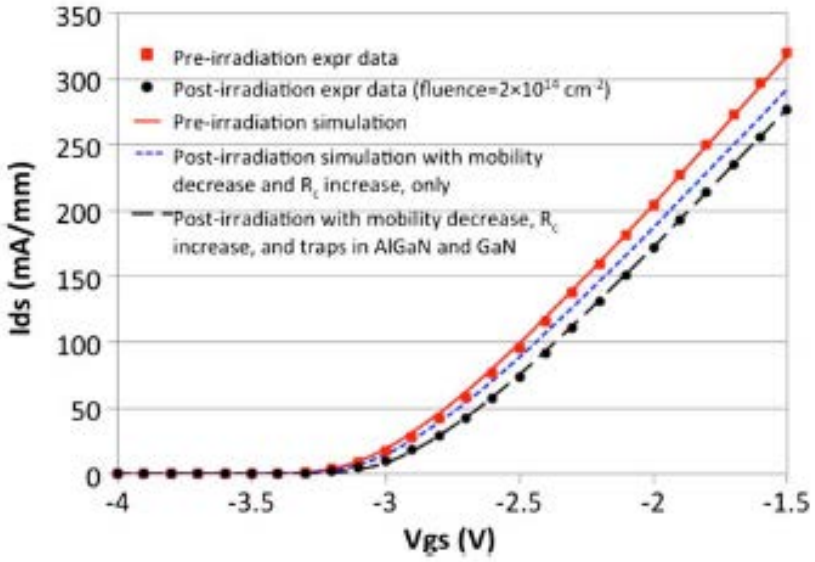

Figure 7. Proton irradiation (fluence 2 $\times 10^{14}$ cm^{-2}) compared with simulation determined that trapped negative charge in the GaN buffer was needed in addition to mobility decrease and R_c increase. The drain to source voltage was reported as 5V. ©[2013] IEEE [18].

fied the need to place trapped charge within 30 nm of the GaN surface to replicate

the threshold voltage shift due to ionization damage caused by 2×10^{14} cm^{-2} 5 MeV protons, as shown in Figure 7. A study conducted by B.D. Weaver et al. mapped the calculated displacement damage dose in the drain current for different ion species and found a degradation starting around 1×10^{11} MeV/g as shown in Figure 8 [27].

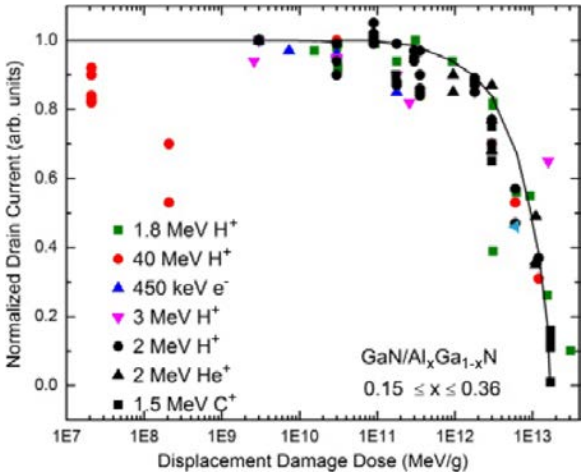

Figure 8. Drain current degradation for different ions at different fluences. ©[2012] IEEE [27].

Additionally, reduction in mobility is associated with ionized impurity concentration increase [4]. Radiation of the center of the gate electrode with 18 MeV Ni ions caused the drain current to increase when ions struck only the center area of the gate and no other region of the device [28]. Kr, Ne or Ar at fluences up to 10^8 cm^{-2} caused permanent damage and identified a new damage mode [29]. Charge collection was observed with Ne and increased leakage current was observed with Ar and Kr [29]. Kr caused a leakage path to occur between the drain and source without any known gate damage recorded [29].

2.3.2 Damage from Neutrons

Neutron interactions with semiconductor devices are of interest to the defense, nuclear reactor and space communities. Neutron interactions in semiconductor ma-

terials can be emulated with ion beams. The concept is that the ion can acts as a

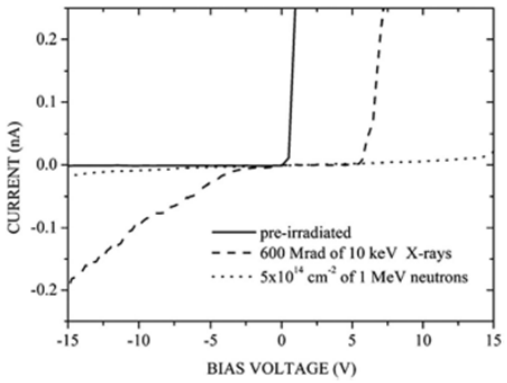

Figure 9. Diode changes affected by neutron damage. ©[2004] IEEE [32].

surrogate to a neutron by creating displacement damage [31]. While the focus of this research was not on neutron damage, some of the information gained in this research may be useful to the neutron community.

Gallium has two stable isotopes (^{69}Ga and ^{71}Ga) which when bombarded with neutrons in a (n,2n) reaction forms stable ^{68}Ga and ^{70}Ga and germanium (^{70}Ge after a B^- decay from ^{70}Ga) atoms [30]. Nitrogen also has a stable isotope, ^{14}N, which when bombarded with neutrons in an (n,2n) reaction forms ^{13}N. The (n,2n) reaction is where one neutron interacts with ^{69}Ga, for example, and ^{68}Ga plus two neutrons are recoiled. With energetic neutrons, the atoms can gain enough energy to become projectile ions within the lattice. One study showed that the diode behavior of the Schottky diode GaN detectors was destroyed after neutron irradiation as shown in Figure 9 [4][32]. Decreases due to 2DEG mobility measured by the Hall Effect showed that mobility decreased rapidly at a certain threshold fluence greatly above which 2DEG conduction was no longer observed [4]. Two traps are associated with donor Ge atoms from neutron irradiation; the total concentration of the 0.45 eV trap and the 0.2 eV trap were correlated to the number of donor Ge atoms from thermal neutron interactions [4].

2.4 AlGaN/GaN HEMTs Irradiated While Bias is Applied

Proton irradiation and applied bias causing high field stress has been explored to determine how the operating bias was affected by proton fluence and how the performance characteristics were changed. It has been shown that the positive threshold voltage shifted more and the normalized peak transconductance decreased more for devices that where held in the high electric field condition known to support hot carriers, V_{ds} = 5V and V_g = -2V [5]. Additional research from Vanderbilt University, correlated defect types and energy to a type of stress such as proton irradiation, high electric field, or semi-on state stress [11]. For example, V_N defects are acceptor defects induced during proton irradiation and can have an energy of 0.25 eV below the conduction band in GaN and 1.2 eV below the conduction band in AlGaN [11]. Where a V_{Ga}-V_N-H_X, where X is 0 to 3, is induced during proton irradiation, high electric field and semi-on state stress can have an energy of 0.6 eV in GaN or 1.1 eV in AlGaN below the conduction band [11].

While increasing proton radiation fluence in the semi-on state, the change in threshold voltage and peak transconductance shift was greater compared to the off state or on state [5]. Low frequency noise measurements were used to identify two traps. The 0.2 eV trap is associated with the N vacancy-related defects in GaN and O_N defects in AlGaN [5] and the 0.7 eV trap was associated with a N_{Ga} defect [5]. Additional coupled proton radiation and applied bias testing in ground state, off state, semi-on state and on state was accomplished and found both total ionizing dose and displacement damage effects [11]. These defects were attributed to the growth process and impurities in the two devices studied; additionally worst-case bias between the two devices differed for the peak transconductance degradation. For the MOCVD grown substrate, the on state condition was the worst-case condition for transconductance degradation [11]. However for the n-type free-standing substrate,

the semi-on condition was the worst-case condition for transconductance degradation [11]. This difference was attributed to the increased defect density at differing observed energies leading to the conclusion that the processing and proton induced defect type and energy distribution are important to consider [11].

2.5 Long Term Reliability Affected by Radiation

Neon, silicon and argon irradiated AlGaN/GaN HEMT commercial devices exhibited no change to DC characterization measurements immediately after irradiation. No change was observed in post irradiation DC or RF characterization either [7]. All three heavy ions were selected with an energy that deposited into the SiC with a fluence on $1x10^5$ ions/cm^2 which simulated a 2 GeV galactic cosmic ray traversing through to a device on the interior of a satellite in a GPS orbit [7]. An elevated baseplate temperature RF stress test comparison between irradiated and non-irradiated devices suggested a possible different degradation rate with long term reliability implications, however, the data was inconclusive [7]. More research is needed to determine how radiation affects long term reliability predictions.

2.6 SRIM/TRIM

The Stopping and Range of Ions in Matter (SRIM) and the Transport of Ions in Matter (TRIM) codes probabilistically describe the interactions of ions with material [33]. SRIM describes the range associated with an ion in another material, or the Bragg Curve determination. TRIM is a Monte Carlo code that describes the probable interactions associated with the ion transport along with all the secondary collisions. Additionally, the composition and depth of each layer of the device is used in TRIM to predict how the device would respond to the ions. Both SRIM and TRIM are needed

to determine what ion, energy and fluence was the best option to cause specific damage at a certain location in the device.

III. Experimental Details and SRIM Calculations

AlGaN/GaN HEMT 2×50 μm devices were irradiated with Ge ions of two different energies at two different locations on the devices. Flux/fluence chosen for this research was not based on realistic mission or space environment. Instead the devices were irradiated to induce degradation and many devices were irradiated to failure. The purpose of this research was not to determine how these devices performed, rather if location based radiation degradation could be measured in situ and what information could be learned from this type of measurement.

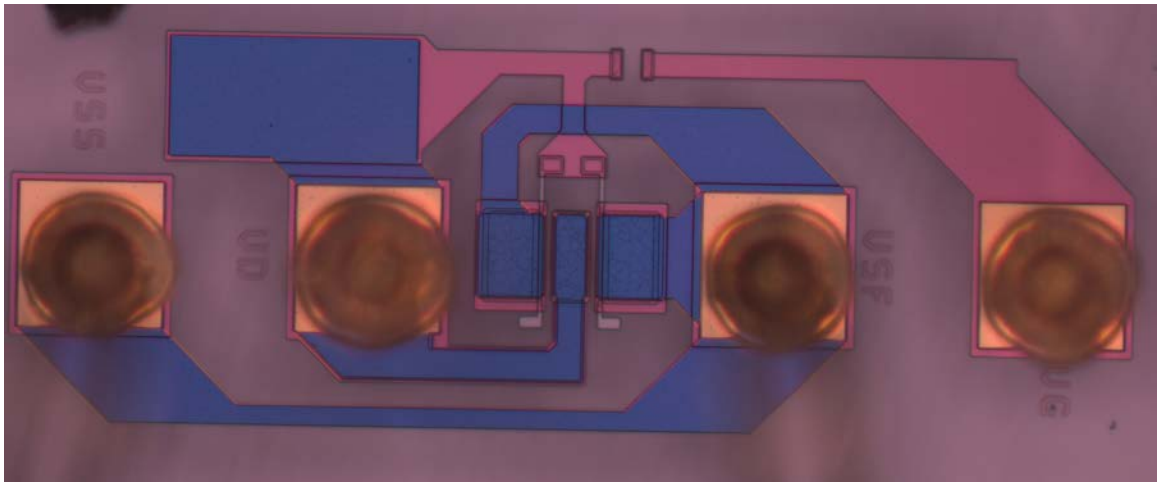

Figure 10. Image of AlGaN/GaN HEMT used in this research at 20x.

3.1 Equipment Setup and Device Description

All devices used during this research had not been used for prior research, however they were manufactured and packaged as commercial-grade test parts designed for the research accomplished by Christiansen in 2011 [2]. The unused devices were stored in a temperature controlled environment for approximately seven years at the Air Force Research Laboratory (AFRL) before being utilized in this research. The

GaN buffer was grown by organometallic vapor phase epitaxy; the AlGaN barrier was not intentionally doped with any additional material [10]. The devices were manufactured with a 0.5 μm t-gate closer to the source than the drain. They also consisted of a GaN cap, a gate-integrated field plate, source connected field plate and SiN passivation which was grown by plasma-enhanced chemical vapor deposition [10], thereby making the design relevant despite the age. Two gates with a width of 50 μm contribute to the output current and are made of a nickel Schottky barrier with thick gold overlay for low gate resistance [10]. The devices were designed to have a built-in capacitor and resistor between the gate and the drain to help with ringing. Each die consisted of two devices, one with a capacitor and the other without. The die was packaged onto Stratedge 580274 packages and the device with the capacitor was wire-bonded to that package as shown in Figure 10. The source was wire-bonded to the backplate of the package, the gate was wired to the top middle lead and the drain was wired to the bottom middle lead. For this research, images were taken of each device to verify the wiring was as described. Prior to use, each package was tested to verify the devices still worked and were statistically within the nominal performance threshold. There was an average positive threshold voltage shift of 1 V noted between 2011 and 2018 (approximately -4 V to -3 V) due to the devices sitting on the shelf. Because the shift was consistent among all the devices, it was decided that the set would be able to provide consistence performance during this research, therefore they were chosen as the devices to be used.

The HVE 6 MV Tandem Accelerator's Micrometer Resolution Optical, Nuclear and Electron Microscope (Micro-ONE) beam was used to irradiate the devices. The devices were mounted to a circuit board which was affixed to an aluminum block. A connector plate was modified to hold the circuit board/aluminum block allowing it to be secured to a structure designed for the vacuum chamber with an onboard PIN

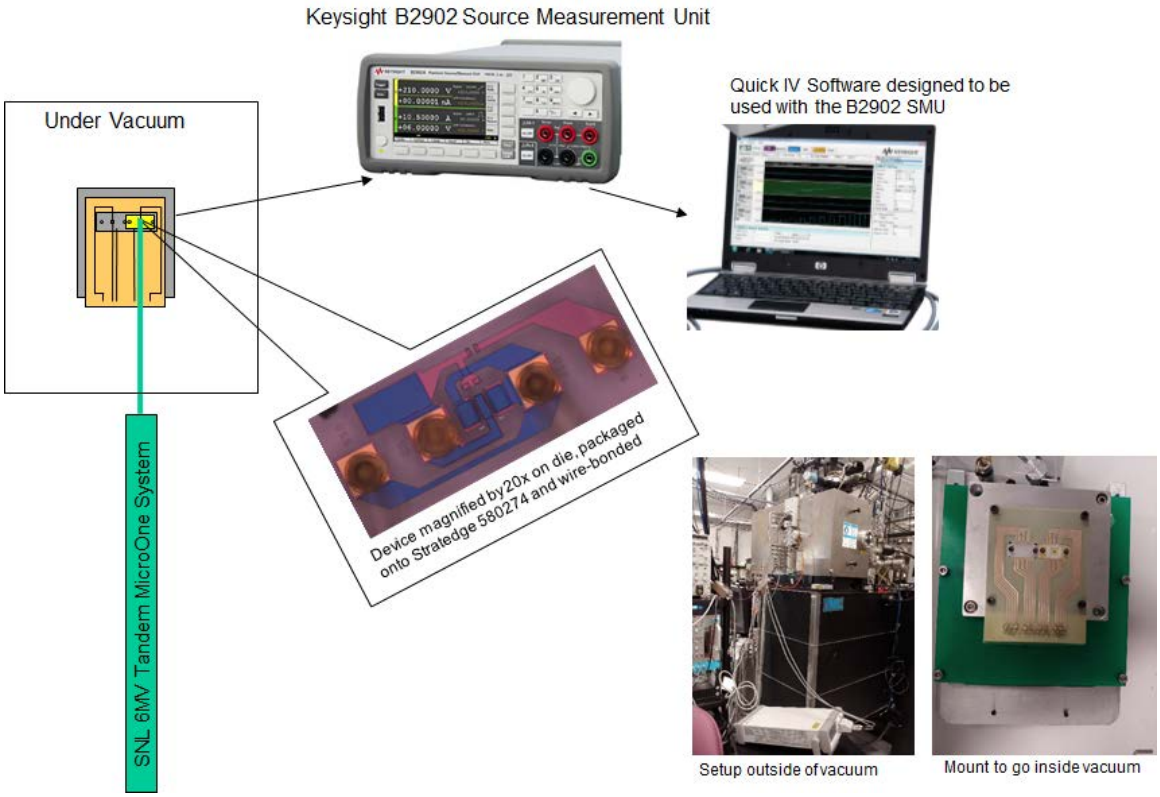

Figure 11. The experimental setup. The ion beam was directed at the specific location of the device and was measured using a B2902 SMU controlled by the computer program Quick IV.

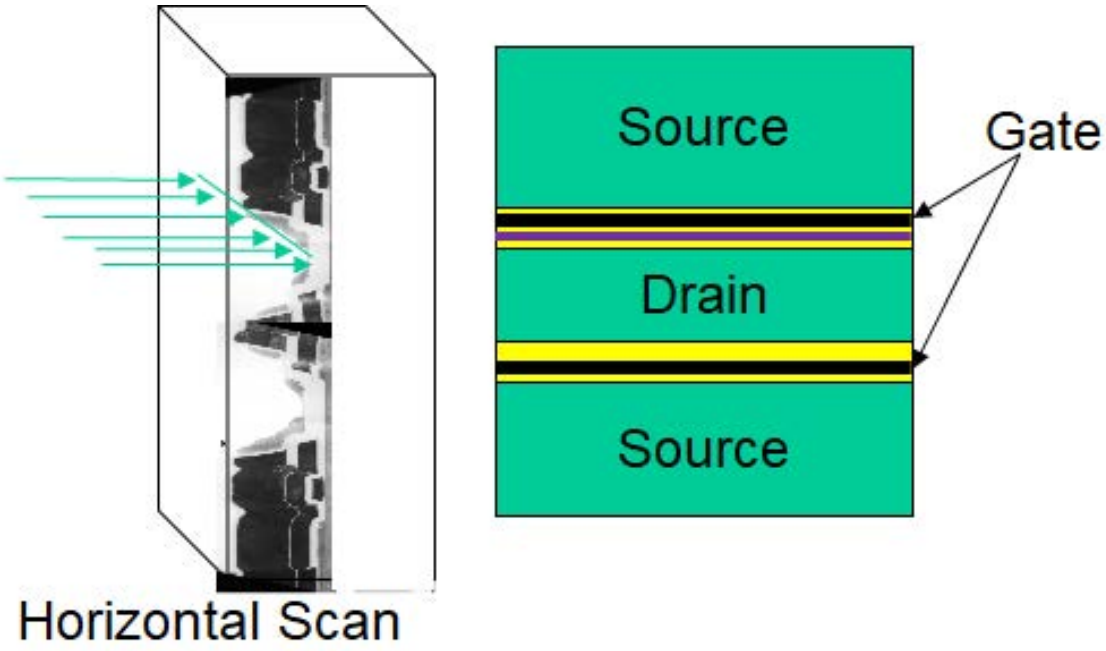

Figure 12. The horizontal scan of ions was accomplished by aiming the ion beam at the target (either the gate-drain gap or the gate) and scanning the length of the device. The purple line correlates to the green arrows, in this case showing the gate-drain gap scenario.

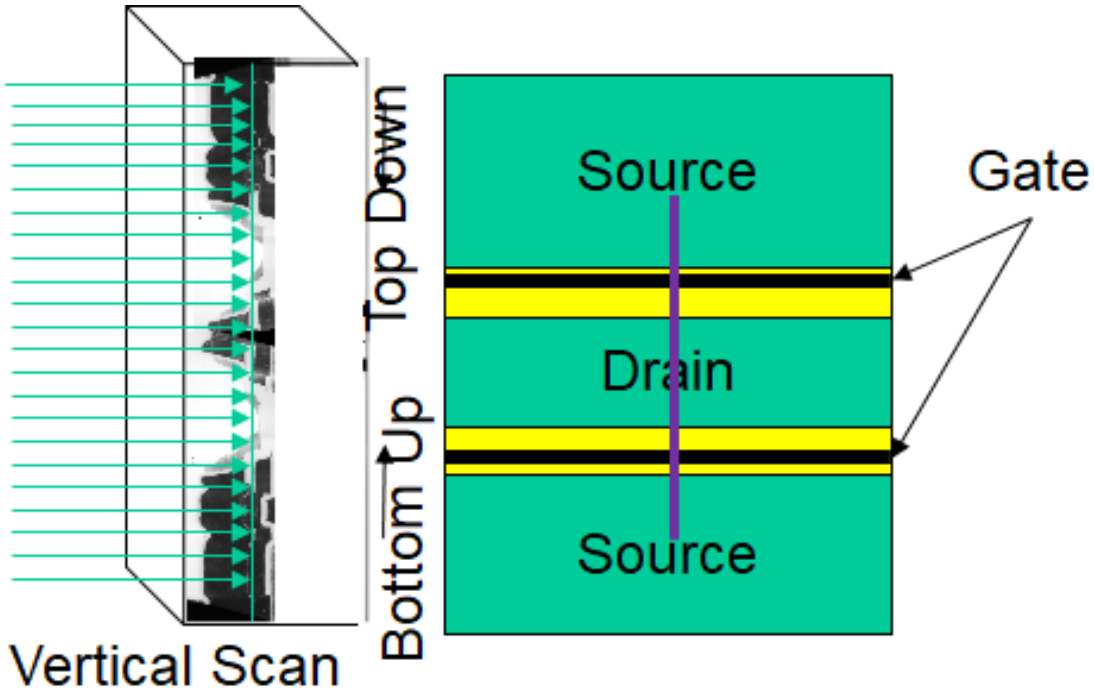

Figure 13. The vertical scan of ions was accomplished by aiming the ion beam at the target and scanning the width of the region from source to source centered on the drain. The purple line correlates to the green arrows.

diode used to measure the ion current. The concept for the circuit board used during this research was created at AFRL for the proton irradiation experiment associated with the 2018 patent application [8]. Pressure and screws connected the leads from the Stratedge package with the gold metal traces of the custom circuit board. The metal trace from the circuit board was soldered to a male db25 connector. The female db25 connector had six wires attached with an SMB connector on the other end of the wire. SMB to BNC wires were used to connect the circuit board through the vacuum chamber to a Keysight B2902A 2-channel Source/Measure Unit (SMU) and the Quick IV software was used to control the SMU at apply current and voltage to the device. A diagram of the setup is shown in Figure 11. The SMU was used for performance characterization and in situ measurements. The devices were very sensitive to ground loops and ringing even with the capacitor and resistor built into the device. To overcome this problem, the SMU was connected to the chamber with a triax to BNC connector on the outside of the chamber using triax cables and connecting to the SMU with triax to banana adapters made by Keysight. During all measurements, the source was common at zero volts. The gate and drain voltage were varied depending on the type of data collected. All measurements were taken at room temperature. The Micro-ONE system created an ion beam that has a spot size of approximately 1 micron depending on which ion energy was used. The ion beam was a Gaussian in space with a full width half max of approximately 1 micron in the x direction and 1.5 microns in the y direction. The ion beam current was inconsistent throughout the day, therefore, the PIN diode was targeted multiple times during the day to assess the current. Each time the ion beam current was measured, the beam was moved to target a different location (away from the device to the PIN diode). This also allowed the targeting accuracy to be validated multiple times a day to ensure

any beam drift was corrected. When drifting of the beam targeting was corrected, the measurements taken with poor targeting accuracy were reaccomplished.

The devices used had two gates with a common drain and separate sources for each gate built in a horizontal plane (not like a vertical Fin Field Effect Transistor (FINFET)) as shown in Figures 12 and 13. During both experiments only one gate region was targeted. When the device was degraded via focused radiation to the point where one of the two gates failed (one finger of the device was irradiated to failure), the combine current reduced to approximately half of the original value which is consistent with one gate being irradiated to failure while the other gate was functional. Because only one gate was irradiated the second gate acted like a built in control when accomplishing DC measurements. While not a true control because the non-irradiated gate region was not independently measurable, it did allow for irradiated devices to be measured even after one gate region was damaged to failure. This is different from broad beam irradiation experiments where the beam irradiates the entire device and both gates of a 2×50 μm device would be irradiated equally.

3.1.1 Targeting Location Rational

Two locations were selected to be targeted with Ge ion radiation, the gate-drain gap and the gate. Two orientations of the ion beam were used during the ion irradiation during this research and are shown in Figures 12 and 13. The horizontal scan was used during both experiments while the vertical scan was only used during the gate experiment.

The gate-drain gap location was chosen to place irradiation near the area that has shown susceptibility to electric-field induced gate leakage current during stress testing [21]. This phenomenon can cause the inverse piezoelectric effect which turns mechanical strain into lattice damage after a critical voltage is applied on the gate

during step stress experiments, the damage is usually located at the drain edge of the gate. Displacement damage from heavy-ion radiation can also cause lattice damage. To use radiation as a tool, the gate-drain gap was chosen to be irradiated with Ge ions with an energy depositing the ions at the interface between the AlGaN and the GaN, to cause displacement damage. Displacement damage causes additional stress on the electric potential between the interface layers, therefore the potential well of the 2DEG could be changed thus reducing the number of carriers in the well, or removing the well completely and therefore reducing the current. Additionally, Ge ions also deposit into the interface region slightly doping the area. During stress testing, a critical voltage was determined to cause gate leakage current to rapidly increase [36]. When drain current degradation was observed to be permanent after stress testing, cracks and pits were determined to be the cause [21]. As the fluence increases, the additional displacement damage should result in the development of mechanical stresses which induce electric fields that can counteract the piezoelectric effect of the interface region. These fields can cause time depended degradation which form percolation paths between gate and channel, electrochemical dissolution which leads to structural damage at the drain edge of the gate and could form cracks and pits. These outcomes are the same as those from the electric field induced gate leakage current failure mechanism observed during stress testing as described in Section 2.1.2.1. Additionally, applied bias has been shown to cause affects when coupled with radiation [5]. Therefore, the gate-drain gap experiment also varied bias to determine how the increasing fluence would be affected by the different bias states changing the electric fields at the interface region.

The gate location was chosen to place irradiation near the area that has shown sensitivity to trapping and detrapping effects during stress testing [20]. Trapping and detrapping effects have led to device drift appearing as changes to threshold voltage

and transconductance. Stress testing has attributed positive threshold voltage shifts to the creation of acceptor traps in the on state and the off state when a high drain current is present. Additionally, the semi-on state caused the worst case positive threshold voltage shift and transconductance reduction when coupled with proton irradiation [5]. The gate experiment in this research used the semi-on condition to test the trap creation caused by ionization damage from Ge ions in the depletion region of the device. The Ge ion energy was chosen to deposit in the SiC substrate reducing the displacement damage at the interface.

3.1.2 Data Collected during Measurements

Optical images of each device were taken at 20x and 50x magnification using an optical microscope at AFIT. Next, pre-irradiation characterization measurements were taken in air at AFIT to make sure the devices still functioned. There were approximately 50 functioning devices that were usable for this research, irradiation of 17 devices are mentioned in this document. The devices were hand carried on an airplane and flown from Ohio to New Mexico. Prior to irradiation, electrical characterization while under vacuum was accomplished to ensure the device was functioning properly as shown in Figure 14. The vacuum pre irradiation measurement is the measurement denoted as 'pre' in later figures in this document.

Pre and post irradiation measurements consisted of collecting the data necessary to generate transfer curves and output current-voltage (I-V) comparisons. The transfer curve held the drain voltage at 0.1V, 0V, 1V, 5V, 10V, 15V, 20V and the gate voltage was swept from -4V to 1.3V in steps of 0.1V; the gate and drain currents were measured. The output curve held the gate voltage at 1V, 0V, -1V, -2V, -3V, -4V, -5V and the drain voltage was swept from -1V to 20V in steps of 0.2V, gate and drain currents were measured. Each measurement sweep was adjusted manually. To

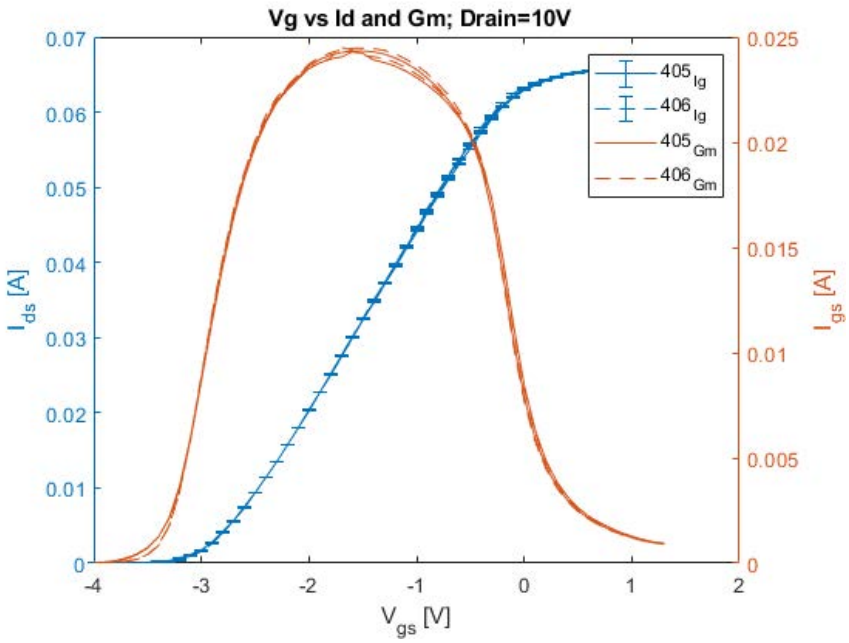

Figure 14. Pre-irradiation measurement of the current-voltage response of a sample of the devices that were used. All were within normal operating performance.

finish the data collection for all the output and transfer curves described above was approximately 10 minutes. In situ measurements applied bias in the off, on and semi-on state. A constant voltage was held on the part before, during and after irradiation for most parts and the change to the gate and drain currents were measured. The off state bias condition held the drain at 5V and the gate at -5V. The on state bias condition held the drain at 5V and the gate at 1V. The semi-on state bias condition held the drain at 5V and the gate at -2V. The threshold voltage for these parts was measured to be -3.1V by using the second-derivative method to extract the value. In addition to data for transfer and output measurements, data measurements where the drain and gate current were held at a constant state were taken pre and post irradiation.

3.2 SRIM/TRIM Material Layer Determination

SRIM/TRIM calculations were used to determine the type and energy of ions to maximize energy deposition in the targeted region [33]. The device used was cross-

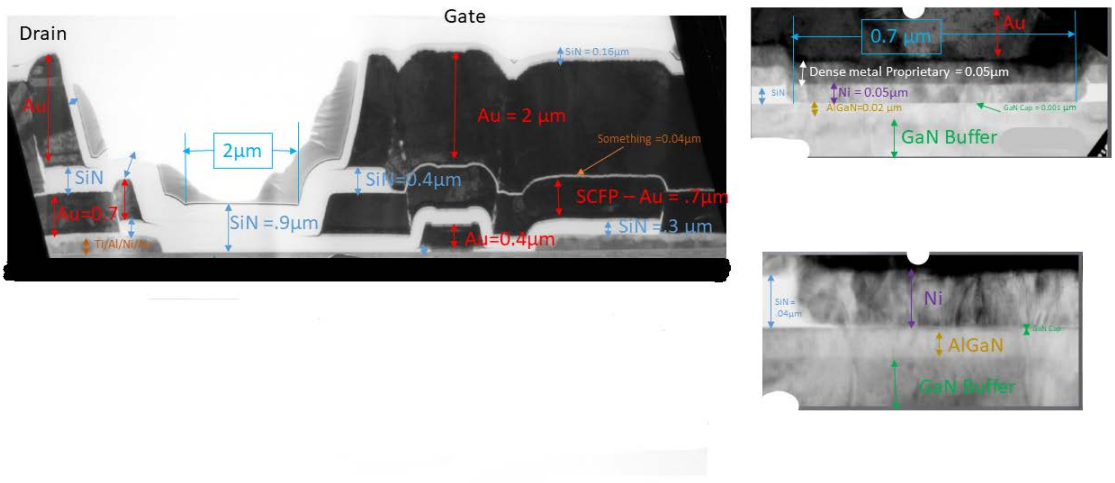

Figure 15. TEM cross-section of device used in research with dimensions.

sectioned using a Transmission Electron Microscope (TEM) in 2011 [13]. Though the chart was not in Christiansen's dissertation it was in his laboratory notes and subsequent research [2]. Using this image allowed determination of the approximate dimensions of the device and thickness of materials as shown in Figure 15. Collaboration with AFRL identified the layer composition based on knowledge of how the device was manufactured, no additional material compositional analysis was used to determine specific thicknesses or validate materials presented in the Figure 15. For the purposed of SRIM/TRIM, the 'Dense proprietary material' was simulated as a thin layer of platinum.

3.3 Displacement Damage - Targeting the Gate-Drain Gap

The gate-drain gap experiment input into TRIM for the transport calculations is shown in the bottom-left of Figure 16. The ions were simulated to impact perpen-

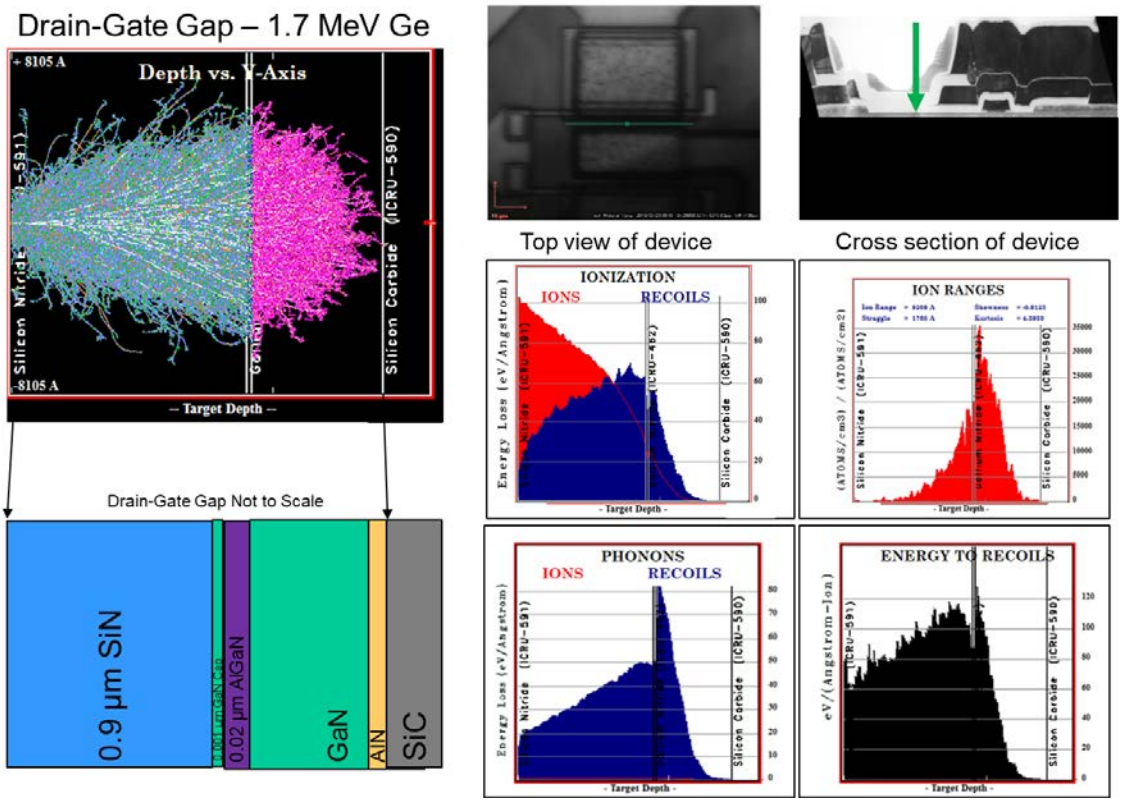

Figure 16. TRIM outputs of gate-drain gap simulation. The top-left chart show the Depth vs. Y axis spread of the Ge ions through the material stack shown in bottom-left. The top-middle and top-right charts show where the irradiation is targeted. The Quad-chart (bottom-right) show various TRIM output charts: Ionization vs Recoils, Ion Range, Phonons and Energy to Recoils.

dicularly to the surface. Multiple ions and energies were run through the simulation to determine which ion and energy combination deposited the most energy at the interface. 1.7 MeV Ge ion provided the best ion range when targeted through the gate-drain gap material as shown in middle-right (top-right of Quad) of Figure 16. The simulation showed that at the 2DEG, the amount of energy loss from recoils was approximately twice that from ionization as shown in the middle (top-left of Quad)

of Figure 16. The distribution of the type of ion being recoiled is shown in Figure 17. The energy loss due to recoils caused by the 1.7 MeV Ge ions will create an environ-

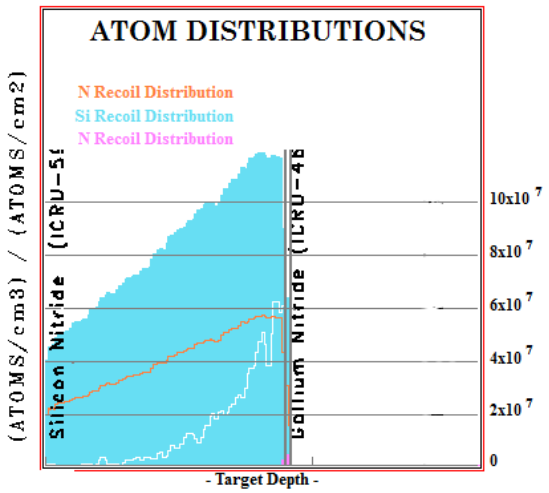

Figure 17. TRIM of the 1.7 MeV Ge ion through the gate-drain gap ion recoil distribution.

ment in the device that should result in observable effects of displacement damage at the 2DEG between the gate and the drain.

The Micro-ONE system on the HVE 6 MV Tandem Accelerator at Sandia National Laboratories Ion Beam Laboratory was used to perform multiple 50 μm horizontal line scans along one finger at the gate-drain gap location of a 2×50 μm AlGaN/GaN HEMT device as shown in the top-middle and top-right of Figure 16. Ten devices were irradiated with an average ion current of 1850±43 ions per second in the drain-gate gap using 1.7 MeV germanium ions. The ion current ranged from 1100-2900 ions/s during irradiation. Three devices were irradiated in the on state, three devices were irradiated in the off state and four devices were irradiated in the semi-on state as shown in Table 1. Measurements inside the vacuum chamber were made while the beam scanned the device, and the ion source was shut. This was to take a background current measurement of the gate and the drain to validate the observed changes were due to the ions and were not an artifact of the system.

Table 1. Gate-Drain Gap - 1.7 MeV

Device	Off	On	Semi-On
2655-0002 (502)			x
2655-0003 (503)	x		
2655-0006 (506)		x	
2655-0007 (507)			x
2655-0010 (510)	x		
2655-0011 (511)		x	
2655-0012 (512)			x
2655-0013 (513)		x	
2655-0017 (517)	x		
2655-0025 (525)			x

The steps that were accomplished for the gate-drain gap experiment were:

1. Electrical characterization in air and optical images.
2. Electrical characterization in vacuum.
3. In-situ data collection of constant bias (either on, off or semi-on) while 1.7 MeV Ge ions are targeted at one of the gaps between the gate and the drain (the other gap/gate was not irradiated).
4. Post-irradiation electrical characterization in vacuum.
5. Optical images if necessary.
6. Electrical characterization after a room temperature anneal for 30 days and 90 days or 210 days.

3.3.1 Semi-On State Devices Example Experimental Timeline

To showcase the type of process each device underwent, the semi-on state of the gate-drain gap experiment will be discussed. The semi-on state devices were 502, 507,

512, and 525. Devices 502 and 525 were irradiated in Aug 2018 while 507 and 513 were irradiated in Jan 2019. Each type of measurement accomplished on the parts of interest will be described below.

3.3.1.1 Device 2655-0002

This device is also known as device 525 in this document. The ion current at the time this device was irradiated was 1100 ions/s. The chronological order of irradiations and measurements was:

1. Pre in-vacuum output and transfer data collection (Aug 2018).
2. Semi-on state 1000s irradiation in situ data collection (Aug 2018).
3. Post semi-on state irradiation output and transfer data collection (Aug 2018).
4. Off state 1000s irradiation in situ data collection (Aug 2018).
5. Post off state irradiation output and transfer data collection (Aug 2018).
6. On state 1000s irradiation in situ data collection (Aug 2018).
7. Post on state irradiation output and transfer data collection (Aug 2018).
8. Post 30 day room temperature anneal output and transfer data collection (Sep 2018).
9. Post 210 day room temperature anneal output and transfer data collection (Mar 2019).

3.3.1.2 Device 2655-0025

This device is also known as device 525 in this document. The ion current at the time this device was irradiated was 1100 ions/s. The chronological order of irradiations and measurements was:

1. Pre in-vacuum output and transfer data collection (Aug 2018).
2. Semi-on state 10s irradiation in situ data collection (Aug 2018).
3. Post semi-on state 10s irradiation output and transfer data collection (Aug 2018).
4. Semi-on state 180s irradiation in situ data collection (Aug 2018).
5. Post semi-on state 180s irradiation output and transfer data collection (Aug 2018).
6. Post 30 day room temperature anneal output and transfer data collection (Sep 2018).
7. Post 210 day room temperature anneal output and transfer data collection (Mar 2019).

3.3.1.3 Device 2655-0007

This device is also known as device 507 in this document. The ion current at the time this device was irradiated was 1250 ions/s and 1300 ions/s for days one and two, respectively. The chronological order of irradiations and measurements was:

1. Pre in-vacuum output and transfer data collection (Jan 7, 2019).
2. Semi-on 180s state irradiation in situ data collection (Jan 7, 2019).
3. Post irradiation output and transfer data collection (Jan 7, 2019).
4. Repeated item 2 and 3.
5. Repeated item 2 and 3.
6. Repeated item 2 and 3.

7. Day 2 pre in-vacuum output and transfer data collection (Jan 8, 2019).
8. Day 2 semi-on state irradiation output and transfer data collection (Jan 8, 2019).
9. Day 2 post irradiation output and transfer data collection (Jan 8, 2019).
10. Repeated item 8 and 9.
11. Repeated item 8 and 9.
12. Repeated item 8 and 9.
13. Repeated item 8 and 9.
14. Repeated item 8 and 9.
15. Post 90 day room temperature anneal output and transfer data collection (Mar 2019).

3.3.1.4 Device 2655-0012

This device is also known as device 512 in this document. The irradiations accomplished on this device were designed to observe the cumulative effect of radiation damage during an in situ measurement. During the first three irradiations, the gold metal over the gate was irradiated by 10^{12} Ge ions. The ion current at the time this device was irradiated was 2420 ions/s. The chronological order of irradiations and measurements was:

1. Pre in-vacuum output and transfer data collection (Jan 9, 2019).
2. Semi-on state irradiation in situ data collection (Jan 9, 2019) - Irradiating Gold Metal.

3. Post irradiation output and transfer data collection (Jan 9, 2019).

4. Repeated item 2 and 3 - Irradiating Gold Metal (Jan 9, 2019).

5. Repeated item 2 and 3 - Irradiating Gold Metal (Jan 9, 2019).

6. Moved 2 microns into gate-drain gap to irradiate (Jan 9, 2019).

7. Post irradiation output and transfer data collection (Jan 9, 2019).

8. Repeated item 6 and 7 - Irradiated gate-drain gap (Jan 9, 2019).

9. Repeated item 6 and 7 - Irradiated gate-drain gap (Jan 9, 2019).

10. Repeated item 6 and 7 - Irradiated gate-drain gap (Jan 9, 2019).

11. Post 90 day room temperature anneal output and transfer data collection (Mar 2019).

3.4 Ionization Damage- Targeting the Gate

Stopping Range of Ions in Matter (SRIM) calculations were used to determine the type and energy of ions needed to deposit the ions in the substrate and cause ionization damage in the targeted region [33]. To compare the the gate experiment with the gate-drain gap experiment, Ge ions were again used, however in order to cause predominant ionization damage in the active region, the energy was increased to 47 MeV. To determine this energy, input into TRIM for the transport calculations is shown in the bottom-left of Figure 19. The ions were simulated to impact perpendicularly to the surface. Multiple ions and energies were run through the simulation to determine which ion and energy combination deposited the most energy at the interface. The 47 MeV Ge ion provided the best peaks at the interface in the Energy to Recoil and Phonon charts when targeted through the gate overlayers and depositing into

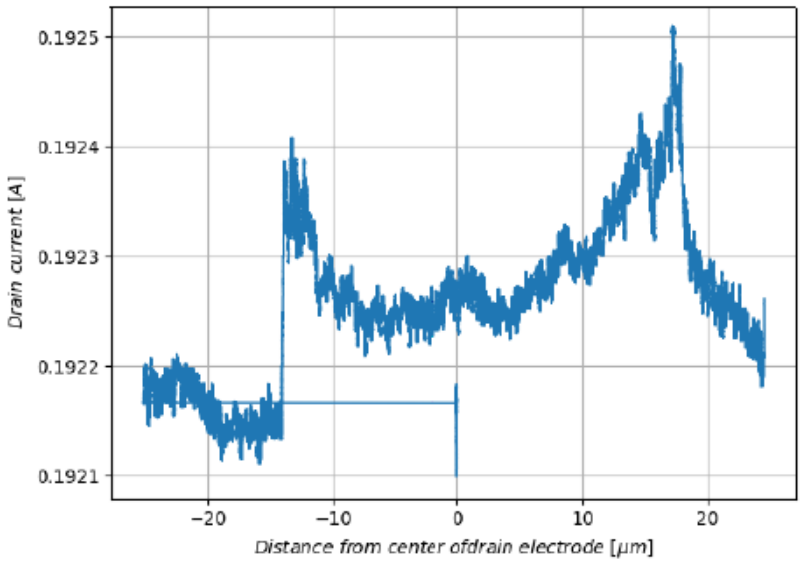

Figure 18. A 5 ms per point vertical scan show the degradation of the drain current is not as clear. The indicates that a slower speed is necessary to produce visible degradation as shown in Fig. 21 [39].

the SiC substrate as shown in bottom-middle and bottom-right of Figure 19. The simulation showed a that at the 2DEG, the amount of energy loss from recoils was insignificant when compared to the amount of energy lost from ions as shown in the middle (top-left of Quad) of Figure 19. The distribution of the type of ion being recoiled is shown in Figure 20. The energy loss due to recoils caused by the 47 MeV Ge ions will create an environment in the device that should enable observation of the effects of ionization damage at the 2DEG between the gate and the drain. This energy also allowed the ions to penetrate through the gate region and deposit in the substrate. The SRIM calculations showed that at the 2DEG, the amount of energy loss from recoils was very small compared to the ionization as shown in Figure 19. This experiment was designed to observe the effects of ionization damage through the gate active region.

The Micro-ONE system on the HVE 6MV Tandem Accelerator at Sandia National Laboratories Ion Beam Laboratory was used to perform 50 μm line scans along one

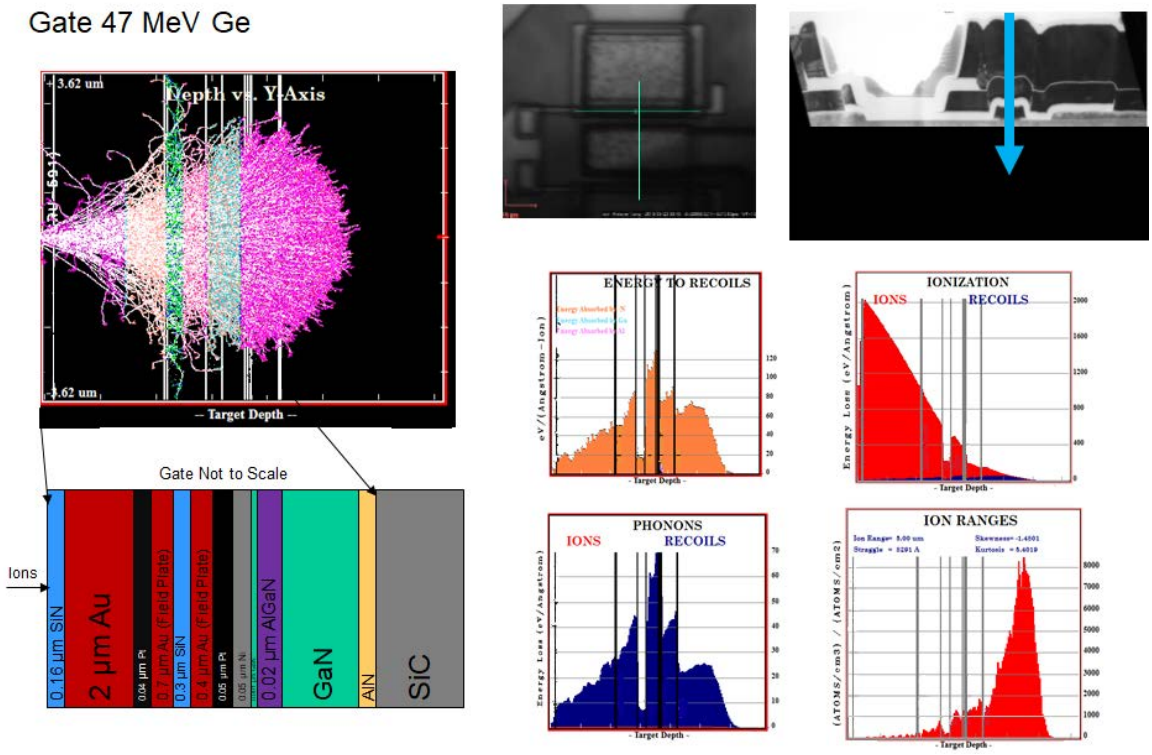

Figure 19. TRIM outputs of gate simulation. The top-left chart show the Depth vs. Y axis spread of the Ge ions through the material stack shown in bottom-left. The top-middle and top-right charts show where the irradiation is targeted. The Quad-chart (bottom-right) show various TRIM output charts: Ionization vs Recoils, Ion Range, Phonons and Energy to Recoils.

finger through the gate of a 2×50 μm AlGaN/GaN HEMT device as shown in the top-middle and top-right of Figures 19 and 19. By only irradiating one gate gap, the secondary gate acted as a control. Seven devices were irradiated with an average ion current of 234±15 ions per second through the gate. The ion current ranged from 100-300 ions/s during irradiation, measured at the sample position by a PIN diode. The average fluence of Ge ions was 2.34×10^{10} cm^{-2}. Control in situ measurements without irradiation were collected to verify that phenomena observed during irradiation was not an artifact of the measurement itself. Four of the seven devices were irradiated multiple times at multiple locations, in an exploratory way using area scan at specific locations. During the exploration, it was observed that the drain current would

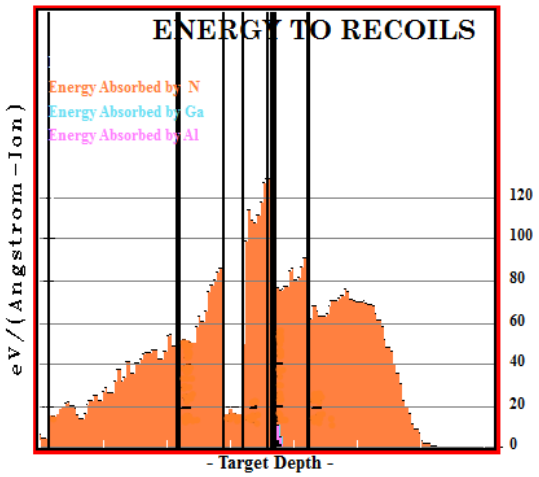

Figure 20. TRIM of the ion recoil distribution of 47 MeV Ge ions through the gate.

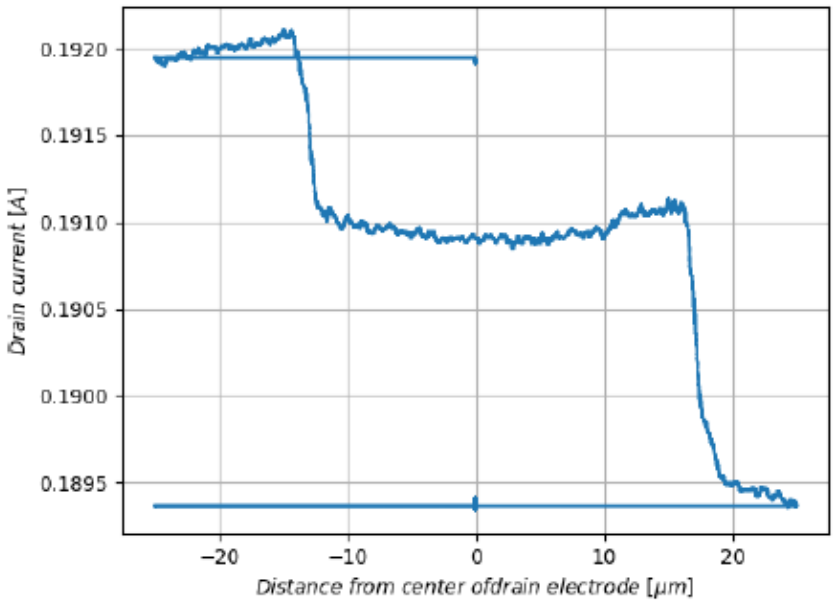

Figure 21. A 50 ms per point vertical scan shows the degradation of the drain current much more clearly than Fig. 18 [39]. These devices have two gates indicated by the current dropping when the ions interact with each of the gate's active regions.

decrease during some area scans. This phenomenon was further explored finding that the 47 MeV Ge ions were interacting with the depletion region, causing the drain and gate current to decrease. To exploit this phenomenon, the three remaining

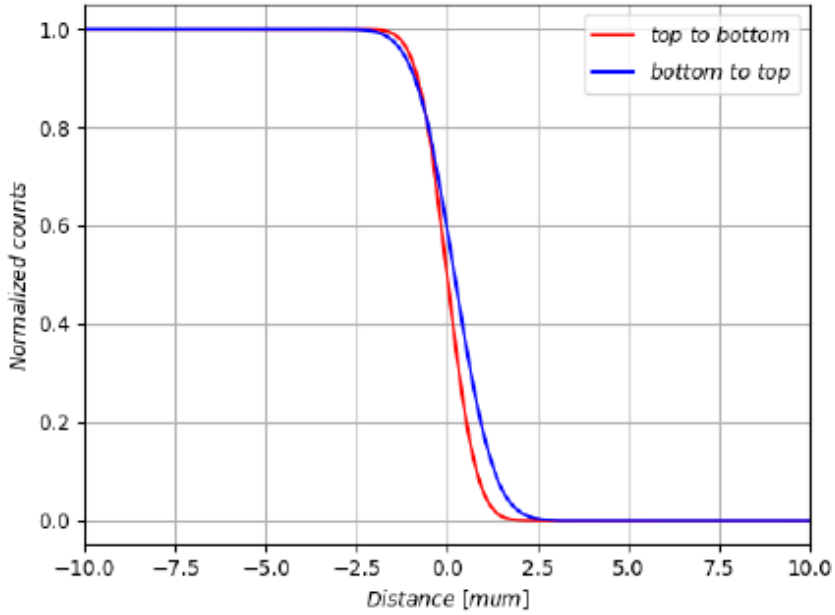

Figure 22. Comparison between the top down and bottom up vertical scans used to find the center of the gate region. The edge is at the same place in both directions and the difference in the midpoints of the fits is 0.24 μm [39].

devices were irradiated using a vertical scan of the ion beam, rather than a horizontal scan. A vertical top-down scan started at the top source, went through the first gate, the first gate-drain gap, the drain, the second gate-drain gap, the second gate and ended at the second source. A vertical bottom-up scan performed the top-down scan in reverse. In each vertical scan, degradation of the current response due to the irradiation and the semi-on state applied voltage was observed twice. Each degradation was observed when the scan interacted with the gate active region. The top-down scan and bottom-up scan were compared and the center of each degradation was located, thereby indicating the center of each of the gate active regions of the

device. A horizontal ion irradiation scan across the device at the gate center location was measured in situ and pre and post-irradiation measurements were compared.

The location of the observed degradation in drain current from the 47 MeV Ge ions was used to target the center of the gate on three devices. An oscilloscope was added to the experimental setup to captured the drain current when the ion chamber opened. The drain current cable to the SMU was split through a 100 ohm resistor to the oscilloscope. The oscilloscope confirmed that the drain current decrease was due to the ions interacting with the gate active region. A vertical scan across both gates using a 50 ms per step using 1000 steps in a line scan showed two regions where the drain current decreased. When accomplished with 5 ms per step, the current degradation was hard to distinguish from the rest of the scan during the in situ measurement to provide inadequate fidelity in correlating the center point of the active region as shown in Figure 18. The larger dwell time per step of the 50 ms per step created the current degradation at each gate to be more spread out, which made finding the center of each gate easier as shown in Figure 21. Two irradiations occurred using the horizontal line scan across a single gate, with the ion beam distribution centered on the middle of the gate as shown in Figure 22.

Six devices were irradiated with 47 MeV ions and one device was used as a control, as shown in Table 2. Three devices were used in an exploratory way where the ionization degradation was observed during area scan measurements. This led to the vertical scan identifying the location of the active gate region followed by the horizontal scan across the gate. The measurements were repeated on both gates of all three devices, so a total of six measurements of the phenomenon was observed.

In Table 2, there are multiple descriptions. Control (no ions) category means that those devices had constant stress but no irradiation was applied and in situ data was collected for output and transfer curves. The semi-on and the off and on categories

Table 2. Gate Experiment Device - 47 MeV

Device	**519**	**522**	**524**	**401**	**404**	**405**	**406**
Date	Jan19	Jan19	Feb19	Feb19	Feb19	Feb19	Feb19
Control (no ions)		X			X		
Semi-on	X		X	X	X	X	X
Off and On	X						
Multi-irradiations	X		X	X	X	X	X
Area	X		X	X			
Vertical Line					X	X	X
Horizontal Line					X	X	X
Isolated Drain					X	X	
Isolated Source					X	X	
Oscope Validation					X	X	X
Two Days			X		X	X	

mean that the devices checked had an in situ irradiation in that constant bias state. Multi-irradiations means that the device was irradiated multiple times and data was collected pre, during and post for each irradiation. This is particularly important for the gate experiment because each gate was targeted separately on devices 405, 406 and 407, so understanding what each irradiation did to the device is important for understanding the radiation induced effects. The Area category indicates devices where a raster rectangular pattern was used; the beam scanned an area that had dimension in the x and dimension in the y as opposed to a horizontal scan where the beam scanned only in the x dimension. Vertical Line and Horizontal Line indicates those devices that were scanned in either a vertical or horizontal line scan, rather than an area pattern. The Isolated Drain and the Isolated Source categories are describing those parts used to irradiate the drain or source using a horizontal line scan. The Oscilloscope (Oscope) Validation category indicates those parts that had the modified gate setup where the oscilloscope was connected to the measurement system. The Two Days category indicates those parts that were left in the vacuum chamber over night; prior to additional irradiations taken on day two, pre-irradiation

measurement data was collected to obtain a new baseline in case annealing changed the device from the previous day.

For the gate experiment, all devices were held at a constant semi-on bias state and drain and gate currents were measured with respect to time during all irradiations. Pre and post irradiation data was collected for output and transfer curves. The sequence of events during the Ionization Experiment was:

1. Electrical characterization in air and optical images.
2. Pre-irradiation electrical characterization in vacuum.
3. 47 MeV Ge ions using area scans encompassing the gate region - Exploration.
4. 47 MeV Ge ions targeted on vertical line scan from source to source - oscilloscope added to setup.
5. Determined location of gate center by comparing vertical scans (scans went from top source to bottom and from bottom source to top).
6. 47 MeV Ge ions targeted one horizontal line scan at the center of one of the gates.
7. 47 MeV Ge ions targeted a second time at the center of the same gate as above in item 6 using a horizontal line scan.
8. 47 MeV Ge ions targeted one horizontal line scan at the center of the source and the center of the drain.
9. 47 MeV Ge ions targeted one horizontal line scan at the center of the second gate.
10. 47 MeV Ge ions targeted a second time at the center of the same gate as above in item 9 using a horizontal line scan.

11. Post-irradiation electrical characterization in vacuum occurred after items 3-6 above.

12. Optical images if necessary.

13. Electrical characterization after a room temperature anneal for 30 days.

3.4.1 Gate Oscilloscope Example Experimental Timeline

To showcase the type of process each device underwent, the gate experiment for device 405 will be discussed. Device 405 was held in the semi-on state during all irradiations. Pre and post data was collected after each irradiation. Devices 404, 405 and 406 were irradiated in late February/early March 2019. The sequence of irradiations and measurements for each device was:

1. Electrical characterization in air and optical images.

2. Pre-irradiation electrical characterization in vacuum.

3. Vertical line scan - bottom source to top source. 50 s scan, 50 ms dwell, 50 μm vertical, drain at 0 and scan went $\pm$25 μm, with a 300 ions/s current (Feb 28, 2019).

4. Vertical line scan - top source to bottom source. 50 s scan, 50 ms dwell, 50 μm vertical, drain at 0 and scan went $\pm$25 μm, 320 ions/s current.

5. Horizontal line scan targeted the drain. 50 s scan, 50 ms dwell across 50 μm horizontal.

6. Horizontal line scan targeted the source. 50 s scan, 50 ms dwell across 50 μm, horizontal.

7. Vertical line scan - bottom source to top source. 50 s scan, 50 ms dwell, 50 μm vertical, drain at 0 and scan went $\pm$25 μm.

8. Horizontal line scan - Centered on bottom gate. 50 s scan, 50 ms dwell across 50 μm, horizontal.

9. Horizontal line scan - Centered on bottom gate a second time. 50 s scan, 50ms dwell across 50 μm, horizontal.

10. Pre-irradiation from day 2 electrical characterization in vacuum (device was under vacuum without activity for approximately 11 hours) (Mar 1, 2019).

11. Vertical line scan - bottom to top. 50 s scan, 50 ms dwell, 50 μm vertical, drain at 0 and scan went $\pm$25 μm.

12. Horizontal line scan - Centered on top gate. 50 s scan, 50 ms dwell, 50 μm vertical, drain at 0 and scan went $\pm$25 μm, with a 400 ions/s current.

13. Post 30 day room temperature anneal output and transfer data collection (Mar 28, 2019).

IV. Gate-Drain Gap Radiation Displacement Damage

This chapter contains excerpts from the journal article that has been submitted to the *Journal of Radiation Effects Research and Engineering*: M. Mace, J. McClory, E. Heller, J. Petrosky, G. Vizkelethy. "Targeted Ion Radiation of AlGaN/GaN High Electron Mobility Transistors through Gate-Drain Gap"

4.1 Abstract

Ten AlGaN/GaN HEMTs were irradiated with 1.7 MeV germanium ions using the Micro-ONE system on the HVE 6 MV Tandem Accelerator at Sandia National Laboratories. Using the Micro-ONE system enabled targeting of the gate-drain gap of the HEMTs with the ions. In situ measurements captured degradation in the on and semi-on bias conditions after varying levels of ion fluence targeted in the gap region; no change to the off bias condition during in situ measurement was observed. Pre and post-irradiation output and transfer performance measurements, including threshold voltage, transconductance, drain current and gate diode characteristics, were compared and analyzed. Changes to these performance characteristics in the on, off and semi-on bias conditions included decreased transconductance, decreased drain current and changes to the diode characteristics were observed, but with no change to the threshold voltage. A delayed response between the start of the ion irradiation and an increased degradation in gate current was observed for both the on and semi-on state bias. A delayed response between the start of ion irradiation and an increased degradation in drain current was also observed for the semi-on state bias. Immediate degradation to the drain current once irradiation began was observed in the on state bias. These observed changes to AlGaN/GaN HEMT device characteristics

during 1.7 MeV Ge ion irradiation are correlated to similar performance degradation mechanisms observed in previous HEMT reliability studies.

4.2 Results

The devices were irradiated while held at a constant drain and gate voltage. A horizontal 50 μm line scan, as described in Figure 12, was rastered over the same line multiple times to increase fluence. The gap between one of the gate and the drain was targeted visually. The on state and semi-on state in situ irradiation is shown in Figures 23 and 24 which capture a representative example of the real time drain current and gate current degradation associated with 1.7 MeV Ge ion irradiation while under bias. While in the off state, the drain and gate currents were insensitive to in situ degradation during irradiation as shown in Figure 25. The black lines on Figures 23, 24 and 25 indicate when the ions were started and when they stopped in relation to when the device began measuring at the constant bias. When the ions interacted with an on state device, the drain current immediately started to decrease; however the gate leakage current did not immediately increase. In the semi-on bias state, the drain and gate currents both had an delay between when the germanium ions interacted with the device and degradation began. Both the drain current and gate current degraded in the on and semi-on state shown in the Figures 23 and 24. The semi-on state irradiation and constant bias began at the same time which did not allow the device time to stabilize. The rate of change of the gate current became steeper after ions were deposited indicating a gate leakage current degradation. Note the gate current becomes more positive in the on state and less negative in the semi-on state when it degrades.

When a delayed response in degradation was present during the in situ measurement it occurred after an average of 5×10^4 germanium ions were deposited in the line

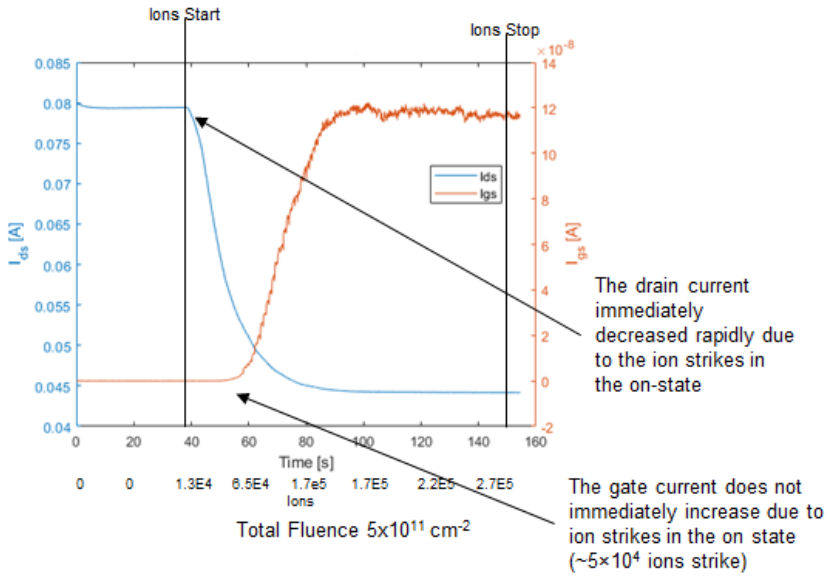

Figure 23. On-bias state during irradiation. Drain current immediately decreased under irradiation, changes in gate current were delayed until a fluence 1×10^{11} cm^{-2}.

scan across the 50 μm gate with a beam width of 1 μm (fluence of 1×10^{11} cm^{-2}). In all bias conditions tested, when the pre and post-irradiation output and transfer measurements were compared as shown in Figures 26, 27 and 28, the post irradiation measurements showed drain current degradation, transconductance degradation and changes to the Schottky gate diode behavior when the drain voltages were 5V or higher. Threshold voltage was not affected because the depletion region under the gate was not targeted. The degradation varied depending on the fluence to which the device was exposed. All three bias states were found to degrade similarly based on fluence in post-irradiation performance measurements.

4.3 Analysis

The electric field induced gate leakage current can cause the inverse piezoelectric effect which turns mechanical strain into lattice damage after a critical voltage is applied on the gate during step stress experiments and the damage is usually at the

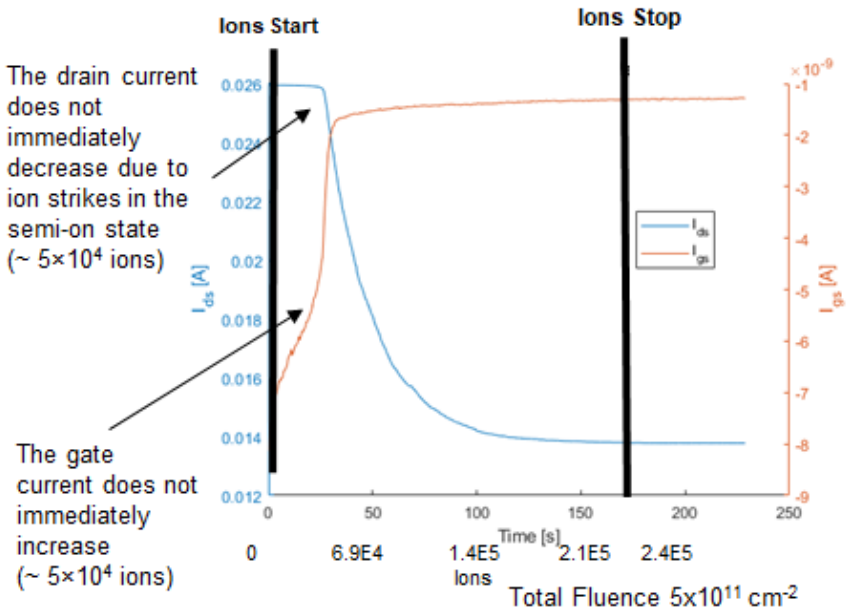

Figure 24. Semi-on state during irradiation. The onset of significant changes in the drain and gate currents occurred at a fluence $1\times10^{11}\ cm^{-2}$.

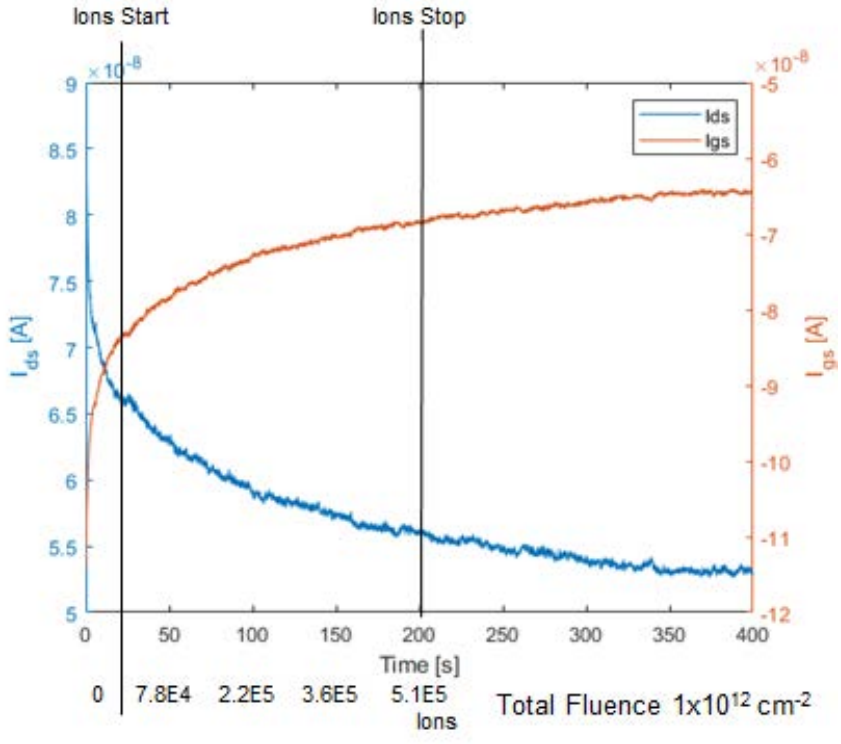

Figure 25. Off state during irradiation. No significant changes to drain or gate current was noted during irradiation.

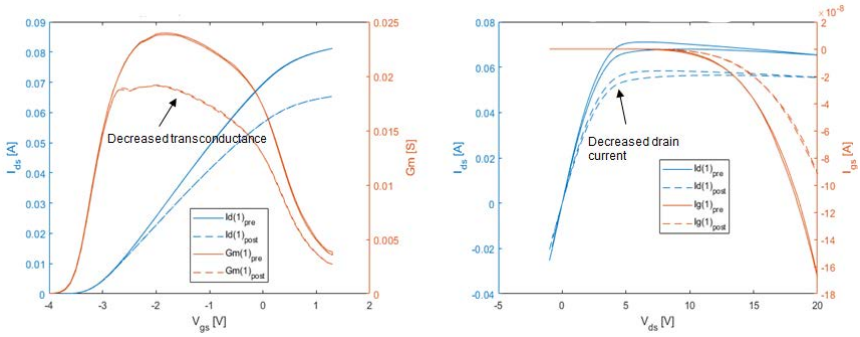

Figure 26. The off state post-irradiation transfer curve where the drain was held at 5V during the measurement (left) and the output curve where the gate was held at 0V during the measurement (right). There was no threshold voltage shift, but drain current and transconductance were degraded.

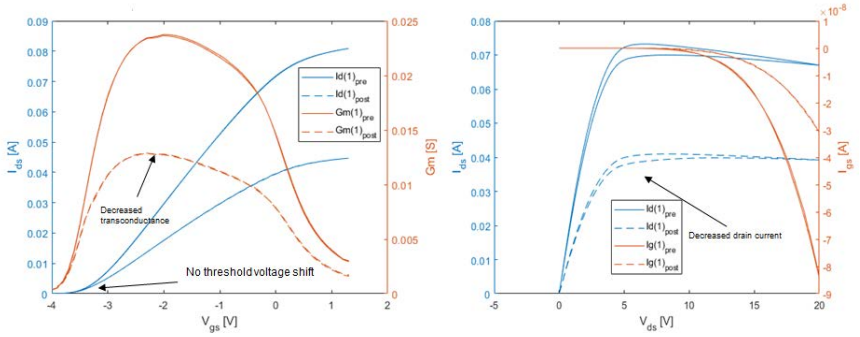

Figure 27. The on state post-irradiation transfer curve where the drain was held at 5V during the measurement (left) and the output curve where the gate was held at 0V during the measurement (right). There was no threshold voltage shift, but drain current and transconductance were degraded.

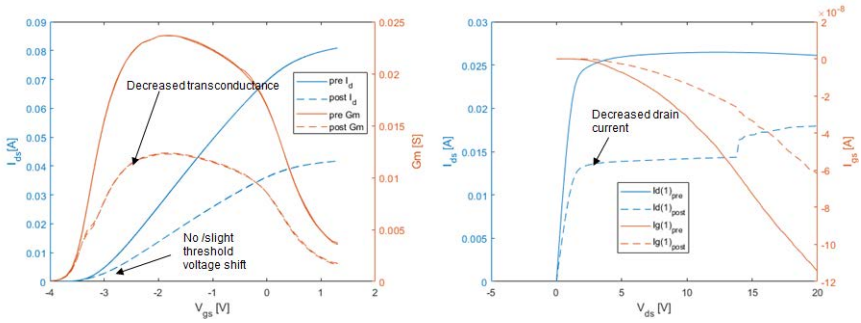

Figure 28. The semi-on state post-irradiation transfer curve where the drain was held at 5V during the measurement (left) and the output curve where the gate was held at -2V during the measurement (right). There was no threshold voltage shift, but drain current and transconductance were degraded.

drain edge of the gate [36]. Additional phenomena associated with gate leakage current degradation during stress tests include time dependent gate degradation forming conductive percolative paths between the gate and channel and electrochemical gate degradation caused by oxidation at the drain edge of the gate [21]. Permanent damage from stress testing has been found to be caused by erosion and cracks in the epitaxial regions [35]. Displacement damage from germanium ions also can cause lattice damage. A delayed response to irradiation was observed in the on and semi-on gate current and in the semi-on drain current which shows that irradiation damage is bias dependent. A similar phenomenon was observed during stress testing by Joh and Del Alamo where they found the V_{DGcrit} was bias dependent and attributed this to the impact of the strain field produced from the source side of the device [37]. A critical fluence causes the gate current to degrade at a certain value and causes the drain current to degrade differently based on bias. Both of these phenomena have been linked with a critical voltage [37]. More research is needed to solidify the link between critical voltage and critical fluence to determine how radiation can be used as a tool to benefit the reliability community.

The ion damage was cumulative as shown in Figure 29. One device was irradiated in the semi-on state targeting the metal contact over the gate and the gate-drain gap multiple times. First, the gate metal was targeted. After three irradiations a total fluence of 2×10^{12} cm^{-2} was deposited in the gate metal. Post-irradiation performance characteristics were not substantially affected because the 1.7 MeV Ge ions did not have enough energy to penetrate to the semiconductor active region. The pre and post-irradiation transconductance measurements associated with Figure 29 are shown in Figure 30. Next the gap between the gate and the drain was targeted. The first measurement of the gate drain gap location is indicated by the blue line in Figure 29 and the circle-line for the drain current and transconductance in Figure 30. The

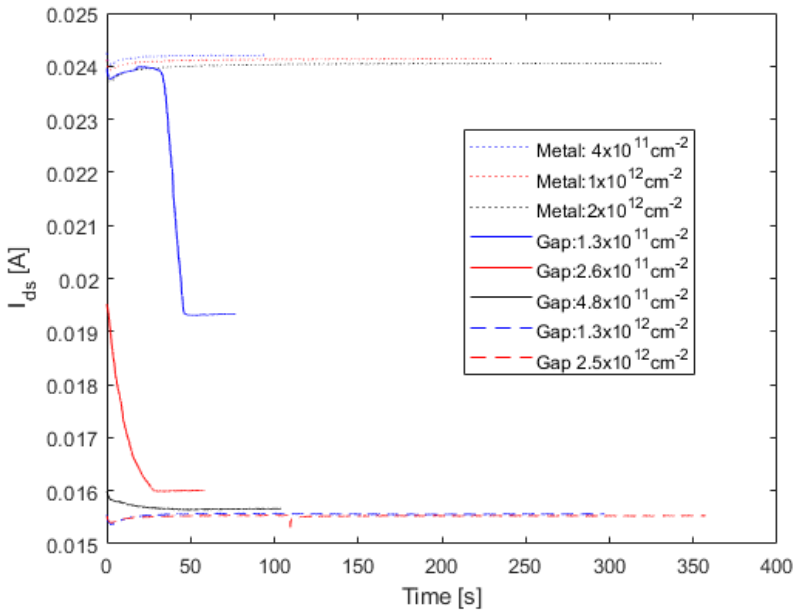

Figure 29. The effect of the radiation is cumulative. When 1.7 MeV Ge ions irradiated the metal over the gate/source area, little change was observed during the in situ measurement. Data from three irradiations in the metal was collected and there was little change in the drain current after a cumulative fluence of 2×10^{12} cm^{-2} indicated by the final Metal label. The fluence labels start over between the Metal and the Gap irradiation locations. A delayed response was observed when the device is targeted in the gate-drain gap where the drain current decreased rapidly as shown by the blue line labeled Gap: 1.3×10^{11} cm^{-2}. Each subsequent label in the legend labeled 'Gap' indicates the cumulative fluence the gap location has received at the end of another round of irradiation and measurements.

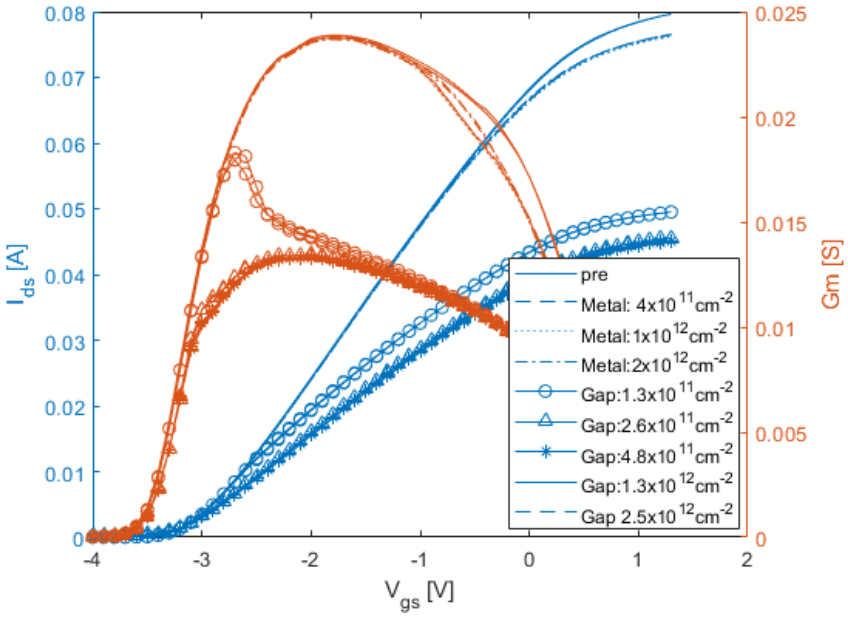

Figure 30. Transfer and transconductance curves post-irradiation shown in Fig. 29. The transfer curves (blue) show little to no threshold voltage shift and the transconductance curves (red) show a decrease. The circle-line for both the transfer and transconductance curve corresponds the blue-line in Fig. 29 (Gap: 1.3×10^{11} cm^{-2}).

delayed response is observed in Figure 24 and was also observed in Figure 29. When the ions were removed, the drain current flattens and does not continue to degrade. The gate current shown in Figure 31 degraded only during the first gate-drain gap irradiation (corresponding to blue line in Figure 29), the remaining gate-drain gap irradiations did not show a change in the gate current.

The irradiation in a semi-on state was repeated and the fluence values shown in the legends of Figures 29 and 30 are cumulative. The second gate-drain gap irradiation did not have a visible offset between ion impact and the drain current degradation. Additionally, the drain current did not recover and started to degrade at the same current level as the end of the previous irradiation. This is an indication of displacement damage. In situ measurements in the semi-on state were repeated until the finger of the device was no longer functioning, noted by the drain current reduction by approximately 50% reaffirming the radiation is only interacting with one

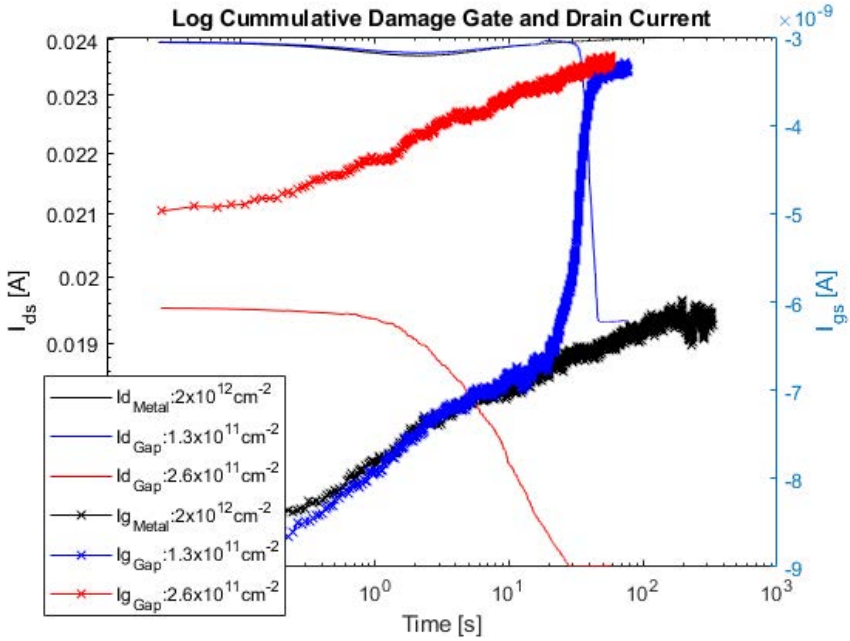

Figure 31. A semi-log representation of time along the x axis showing the gate and drain current degradation. The black lines are when the 1.7 MeV Ge ions were targeted over the gold metal above the gate. The blue line indicates the first time the gate-drain gap is irradiated with multiple line scans depositing 1.3 MeV Ge ions/cm^{-2} in this specific location. The red indicates the second time the gate-drain gap is irradiated with multiple line scans causing an additional 1.3 MeV Ge ions/cm^{-2} fluence to interact making the cummulative damage in the area 2.6 MeV Ge ions/cm^{-2}. Solid lines indicate the drain current which follow the left axis and the x lines indicate the gate current which follow the right axis.

of the two gates. The transconductance after the gate-drain gap was irradiated the first time with a cumulative damage of 1.3×10^{11} cm^{-2} has a kink during measurements with drain voltages 5 V as shown in Figure 30. This kink was also observed when drain voltages were greater than 5 V during the measurements. This was likely caused by the non-linearity of the drain resistance compared to the source resistance and is more noticeable for the higher drain voltages measurements [38]. The resistance was likely increased due to the displacement damage in and around the 2DEG created by the Ge ions and the subsequent recoils that occurred in the lattice atoms between the gate and the drain, increasing scattering and thus reducing the mobility. This is a similar effect that has been observed in stress testing causing an inverse piezoelectric effect from mechanical strain causing defect damage to the lattice.

Figure 32. Same part pre-irradiation (left) and post-irradiation (right). The burn mark (blackened area) appeared during post-irradiation in the on state output measurements, when the gate voltage was held constant and the drain voltage was swept from 0 to 20V.

The transfer curve measurements, i.e. varying the gate voltage with a constant drain voltage, were recorded first during the post-irradiation measurement and both the on state or semi-on state devices responded as expected. However, when the output curve measurements were initiated, i.e. varying the drain current with a constant gate voltage, some of the on state and semi-on state devices responded with large

gate currents. When output data was measured for the on state devices, one of the three devices burned out as shown in Figure 32. When the output data was measured for the semi-on state devices, two of the four devices caused the measurement system to hit compliance and cease recording data.

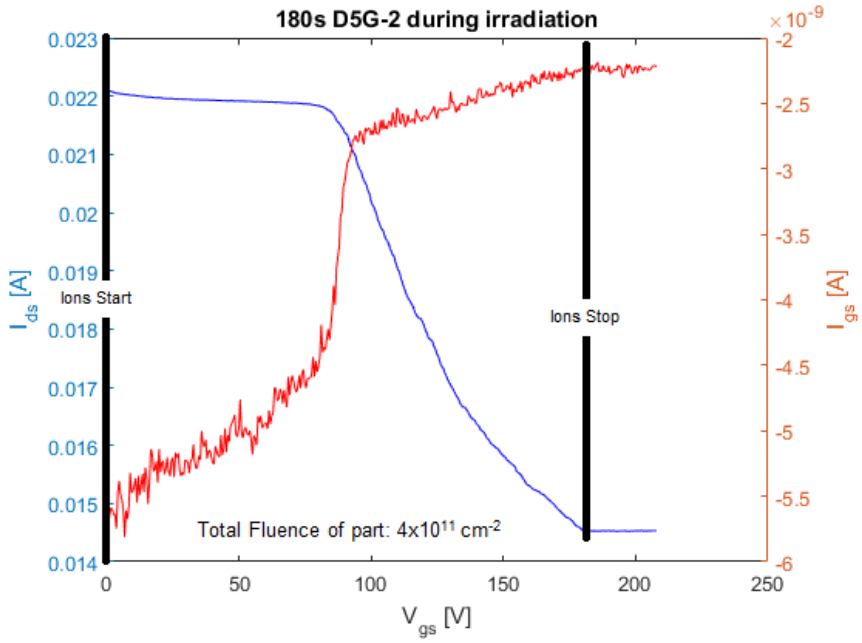

Figure 33. Semi-on state device 525 was irradiated as described in Section 3.3.1.2. This is the in situ data collected during irradiation for 180s.

Device 525 was discussed in Section 3.3.1.2, the 180 s in situ data of the drain and gate current is shown in Figure 33. Post-irradiation measurement of this device showed that the drain current recovered after a 30 day room temperature anneal, as shown in Figure 34. Figure 34 also shows how the gate diode characteristics were changed due to the irradiation and then almost fully recovered after the 30 day room temperature anneal as well. The device that recovered had both delayed drain and gate current degradation; the drain current flattened in a similar manner to that observed in the first gate-drain gap irradiation during the cumulative damage experiment as shown in Figure 29. However, during the actual data collection of

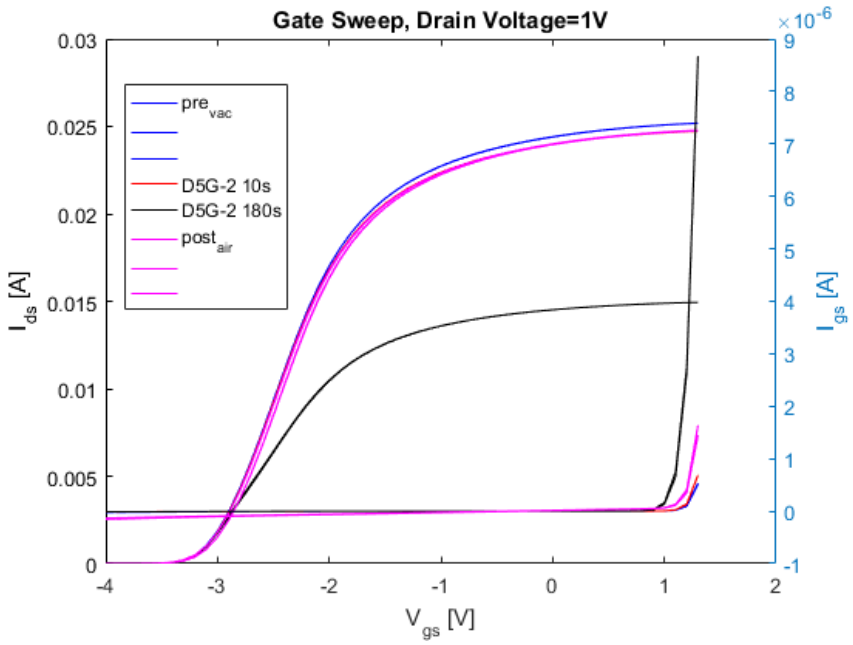

Figure 34. Post 30 day anneal measurements compared to all measurements described in Section 3.3.1.2. The gate current diode behavior nearly recovers after 30 day room temperature anneal (pink).

additional post-anneal measurements this device failed to turn off. Most of the devices were irradiated until the finger of the device was no longer functioning, therefore the exact conditions necessary for recoverability from ion damage in the gate-drain gap is unknown.

Electrical stress and proton irradiation induced defects have been correlated by [11]; who also noted that an on state bias may enhance different defects than those produced when an off state bias is applied. Semi-on state stress and proton irradiation have been correlated to cause the same defects [11]. More research is required to determine the cause of the offset of the drain current degradation in the semi-on state versus its immediate degradation in the on-state as identified in this research. It could also be due to both the on state bias and the germanium ion irradiation causing the same defect (V_N perhaps) thereby increasing the degradation associated with that defect immediately. The semi-on bias and the germanium ion irradiation

does not immediately create the same defect, instead it takes time for the increased number of those defects to be created (V_{Ga}-V_N-H_x perhaps).

4.4 Conclusion

Irradiating through the gate-drain gap in the on, off and semi-on bias conditions caused significant reduction in transconductance, and changes to gate diode behavior. There were no changes in the threshold voltage noted for the on, off or semi-on bias states. Increased gate current and decreased drain current was observed during on and semi-on states when measured in situ with 1.7 MeV Ge ion irradiation. In the semi-on state and on state a fluence of 1×10^{11} cm^{-2} was a representative critical fluence observed to increase gate current. This same critical fluence was also observed to decrease drain current when irradiated in the semi-on state. However, in the on state, the drain current degradation was immediately observed. The direct cause of the different behavior of the drain current degradation between the semi-on state and on state bias when coupled with 1.7 MeV Ge ions targeted in the gap between the gate and the drain is unknown at this time. Overall, targeted irradiation along the gate-drain gap appears to replicate similar performance characteristic degradations observed in reliability studies of AlGaN/GaN HEMTs. Further research using this technique may help both the reliability and radiation effects communities to better understand failure mechanisms within AlGaN/GaN HEMTs.

Using a microbeam to target specific areas of semiconductor devices allowed degradation to be observed in situ under different operating conditions. The observed in situ degradation was correlated to changes in performance characteristics. No threshold voltage shift, for example, indicated that the active region under the gate was not affected in a targeted experiment of the gate-drain gap. The amount of degradation in performance characteristics can be correlated to the amount of radiation damage in a

specific region when using this technique. Defects introduced in and near the 2DEG cause decreases in the 2DEG density and electron mobility which decreases drain current. By using a microbeam to target specific areas of the device, degradation can be captured in situ, helping to pinpoint failure locations as well as validate modeling and simulation software designed to identify device reliability parameters. Improved qualification protocols for radiation and intrinsic reliability can also be informed by using this technique to understand failure limits due to defects and radiation damage.

V. Gate Radiation Ionization Damage

This chapter contains excerpts of the journal article that will be submitted to the *IEEE Transactions on Device and Materials Reliability*: M. Mace, J. McClory, E. Heller, J. Petrosky, G. Vizkelethy. "Targeted 47 MeV Ge Ion Radiation of AlGaN/GaN High Electron Mobility Transistors."

5.1 Abstract

AlGaN/GaN HEMTs were irradiated by targeting 47 MeV germanium ions through the gate active region while the device was held in a semi-on bias state using the Micro-ONE system on the HVE 6 MV Tandem Accelerator at Sandia National Laboratories. Damage was observed during exploratory studies, where the drain current was reduced when the ions interacted within a specific region on the device which was later determined to be the active region under the gate. To exploit this phenomenon, a vertical line scan was accomplished to deposit ions across the source-gate-drain-gate-source in a top-down and bottom-up manner. It was observed that the dwell time of ions during the vertical scan was an important consideration to help identify the active area of the gate; when the scan occurred too quickly the data collected was noisy. The two scans were compared to identify the location of the center of each gate. Then, one gate of the device was targeted using the ion beam to scan horizontally across its length while held in a constant semi-on state bias. In situ data was collected to determine how the gate and drain currents responded to the ions. This was repeated a second time over the same gate. Pre and post irradiation performance characteristics were compared and analyzed. In situ measurements were able to capture drain and gate current degradation caused by the ions. Pre and post irradiation measurements confirmed threshold voltage shifts were due to the gate cur-

rent degradation after the first irradiation likely causing trap formation in the AlGaN or GaN layers of the device. Post 30 day room temperature anneal measurements confirmed damage induced by the ions did not recover.

5.2 Results

An initial irradiation by 47 MeV Ge ions targeted through the gate caused drain and gate currents to degrade due to ionizations in the gate active region. A positive threshold voltage shift was also observed. Subsequent irradiation by 47 Ge ions of the gate region resulted in further degradation of the drain current but no further shift in the threshold voltage, indicating that the threshold voltage shift reached a saturation level.

Targeting the gate region was difficult because the gate length was very small, less than 1 μm and the ion beam was 1 μm wide, therefore optically targeting the gate was not adequate. To determine the exact location of the gates on a 2×50 μm AlGaN/GaN HEMT, the drain current degradation was observed during a vertical line scan, as described in Section 3.4. The vertical line scan did not determine how the rate of current degradation changed at the drain edge of the gate because the ion beam was too wide; the entire gate region was being irradiated. A thinner ion beam is needed to obtain precise information across the gate length. As the vertical line scan swept across the gate length, the distribution of the ion beam caused some ions to hit the active region under the gate contributing to the observed drain current degradation. This, along with the on-board capacitor and resistor, caused the observed drain current degradation to persist beyond the expected gate region. Figure 22 in Chapter III shows that the drain current degradation extends approximately 5 microns, while, the actual gate length is less than a micron. However, the center point can be determined using the methodology described in Section 3.4.

As a representative example, one of the devices described in Section 3.4.1 (device 405) will be discussed. Prior to any irradiation, the data was collected in air to ensure the device was functioning (step 1 of Section 3.4.1). Next prior to any irradiation, data for output and transfer curves was collected under vacuum (step 2 of Section 3.4.1). Vertical line scans, as shown in Figure 35, using the methodology described in Section 3.4 were accomplished to determine the center location of the two gates on the device 405; these correspond to items 3 and 4 described in Section 3.4.1. Next, steps 5 and 6 in Section 3.4.1 were conducted, drain and source irradiation, respectively. The drain was targeted by 47 MeV ions while under a semi-on bias using the single horizontal line scan methodology described in Section 3.4; Figure 36 shows the in situ data for the corresponding drain and gate currents. When the ions interact with the drain, a photocurrent-like response is observed in the drain current; there was no associated change to post-irradiation performance characteristics observed. The source was targeted using the single horizontal line scan methodology as well. The data collected in situ during irradiated under a semi-on bias showed no change to the gate or drain current. No change was observed in the post-irradiation data collected for the output or transfer curves either.

Next, step 7 in Section 3.4, another vertical line scan and in situ measurement to validate the originally determined location of the gates was conducted. There were no observed output or transfer curve changes in post-irradiation data collection for steps 1-7 as shown in Figures 40 and 41. Steps 8 and 9, the first and second horizontal line scan across the bottom gate width, were then conducted. A single horizontal line scan targeted the center of the bottom gate. The device was held in a semi-on bias state and ions were deposited across the width of the channel; in situ data of the gate and drain currents were collected. The ion irradiation caused the drain and gate currents to degrade. The drain current degradation, shown in Figure 37 (blue),

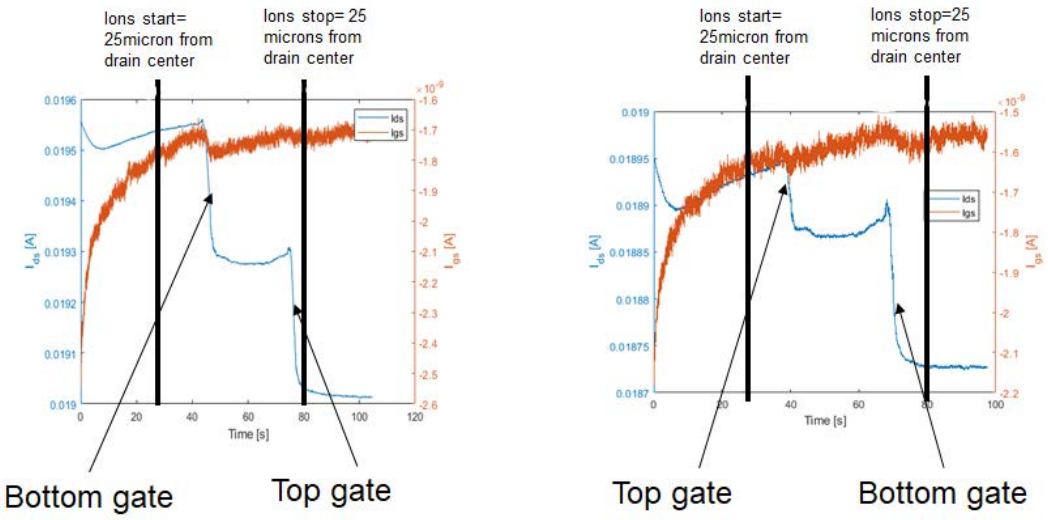

Figure 35. The bottom up (left) and top down (right) scans used to determine the location of the center of each gate on device 405. The blue lines correspond to the in situ drain current while held and a constant semi-on bias condition (Drain =5V, Gate =-2V) while irradiated with 47 MeV Ge ions. The red lines correspond to the gate current during the same irradiation. The black lines indicate where the ions started and where they stopped. The average ion current for both of these irradiations was 325 ions/s.

was continuous as the ions deposited across the entire width of the channel and the drain current degradation stopped when the ion beam stopped. The gate current degradation observed during the first in situ measurement, shown in Figure 37 (red), is correlated to a positive threshold voltage shift and transconductance decrease as shown in Figure 39. The drain current also decreased as a result of the irradiation. During a second horizontal line scan across the bottom gate channel width, the drain current degraded more, however the gate current did not degrade, as shown in Figure 38. The post-irradiation data collected correlated to a decrease in drain current and transconductance, but there was no threshold voltage shift, as shown in Figure 39. This data is also presented in Figures 40 and 41 as lines 8 and 9.

The device was kept under vacuum until the next day (step 10 of Section 3.4). Data was collected for output and transfer curves and no overnight annealing was observed, as shown in line 10 of Figures 40 and 41. An additional vertical scan was

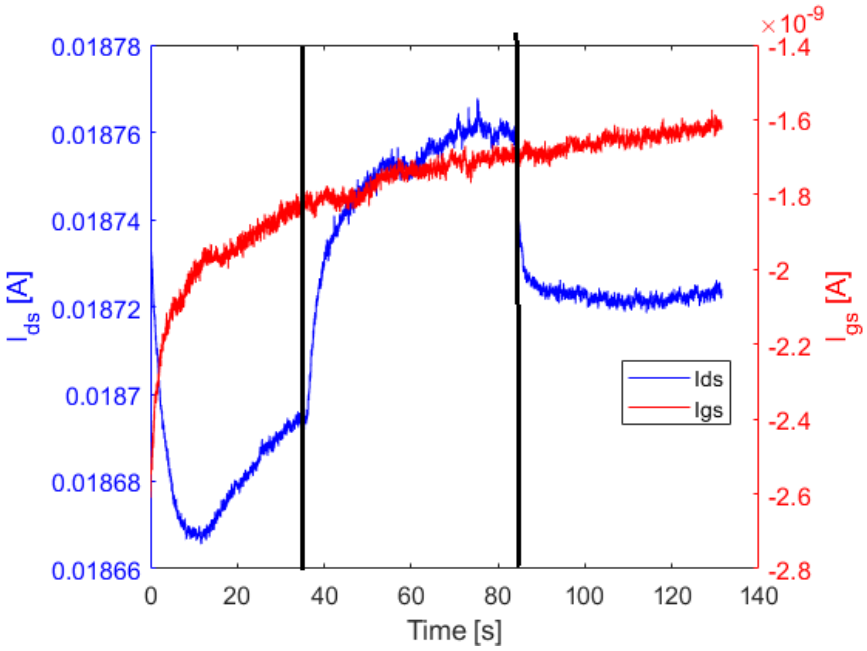

Figure 36. 47 MeV Ge ions targeted horizontally through the drain producing a photo current response.

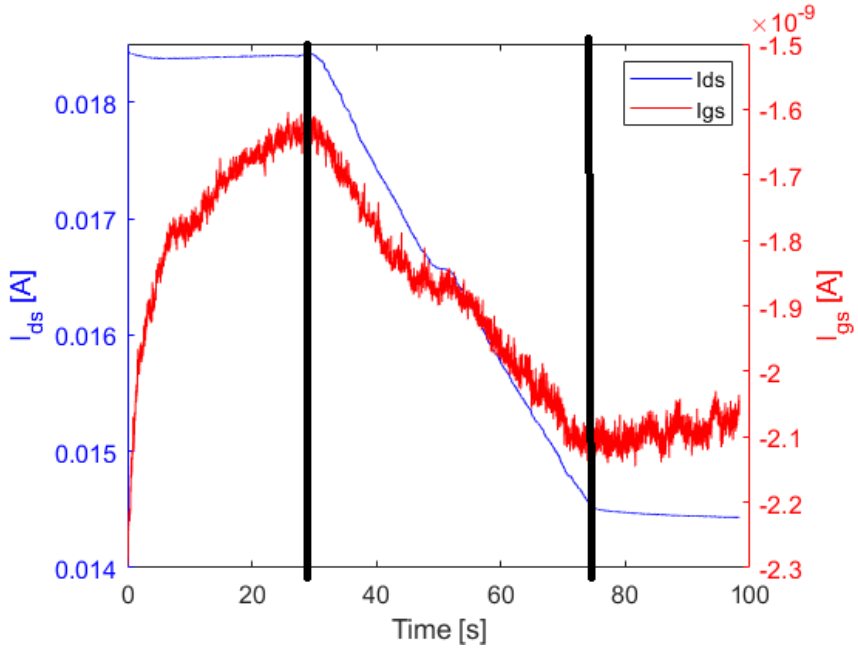

Figure 37. First horizontal 50 μm line scan centered through the bottom gate across an AlGaN/GaN HEMT. The ions started around 25 s and ended around 75 s. This degradation was verified more precisely with the oscilloscope reading which triggered off of the ion beam. The gate and the drain current are both degrading as a result of this irradiation.

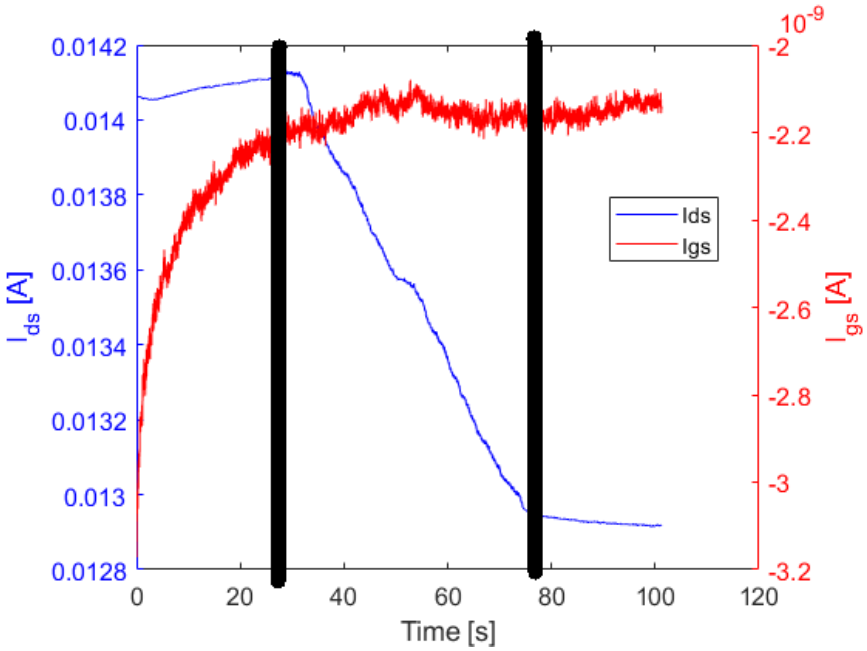

Figure 38. Second horizontal 50 μm line scan centered through the bottom gate across an AlGaN/GaN HEMT. The drain current is degrading as a result of this irradiation, the gate current is not.

accomplished to ensure the location of the gates were known and post-irradiation data was collected for output and transfer curves, as shown in line 11 of Figures 40 and 41 Next, the top gate was irradiated for the first time with a horizontal line scan as described in the steps of Section 3.4.1. The in situ gate current and drain current degraded resulting in the positive threshold voltage shift and decreased drain current observed in Figures 40 and 41. Two additional devices followed a similar irradiation and measurement outline. Each time the threshold voltage shifted, the gate current had degraded during the in situ measurement. After a 30 day room temperature anneal, the degradation persisted indicating permanent damage due to the irradiation as shown in line 13 of Figures 40 and 41.

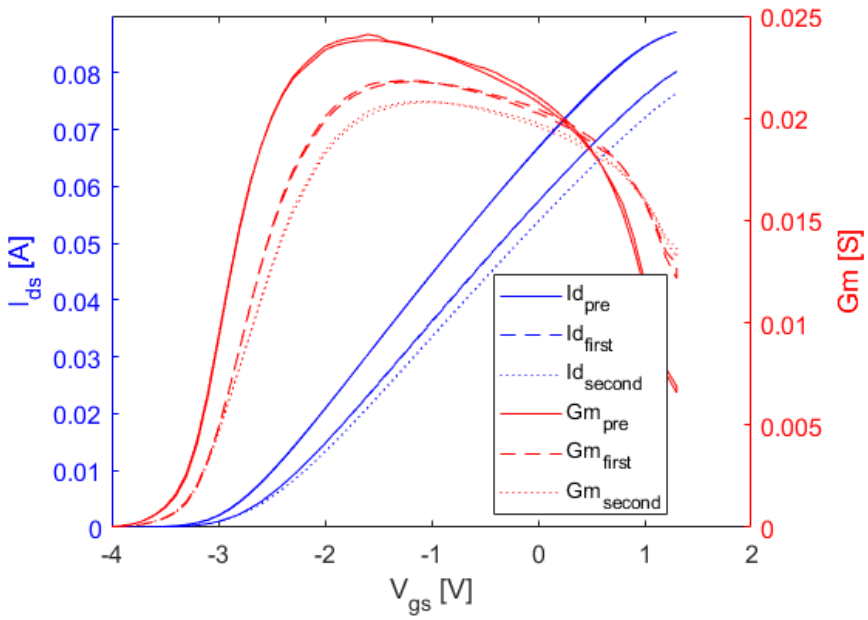

Figure 39. Pre-irradiation and post-irradiation data from gate irradiation. The data sub-labeled 'Pre' in the legend of this figure is the data collected during a post-irradiation measurement of a vertical line scan (step 7 in Section 3.4.1). The in situ measurement of Figure 37 is the data sub-labeled 'first' (step 8 in Section 3.4.1), and the in situ measurement of Figure 38 is the data sub-labeled 'second' (step 9 in Section 3.4.1). First and second corresponds to the first and the second irradiation of the bottom gate, respectively.

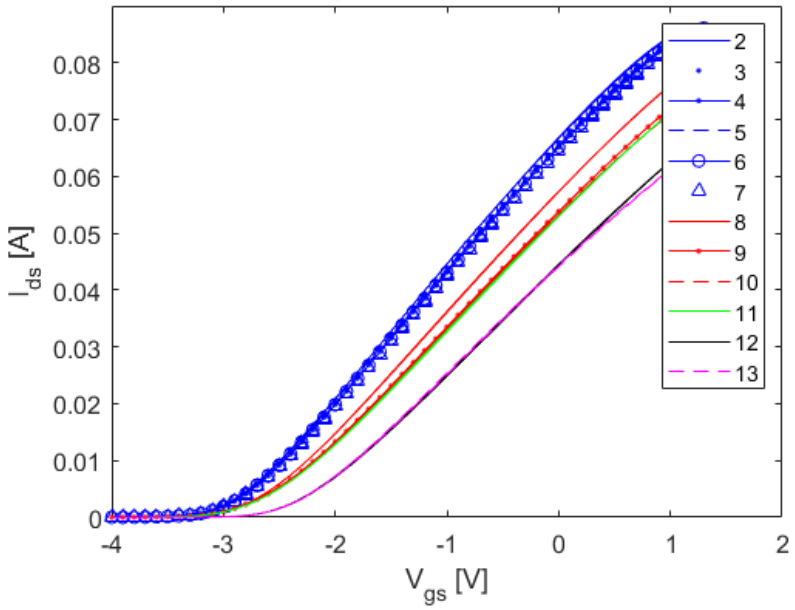

Figure 40. Transfer curve, i.e. drain current as a function of gate voltage where the drain voltage was a constant 15V. The number labels on the data (2-13), correspond with the steps listed in Section 3.4.1. Line 8 indicates the first horizontal line scan across the bottom gate and line 12 indicates the first horizontal line scan across the top gate.

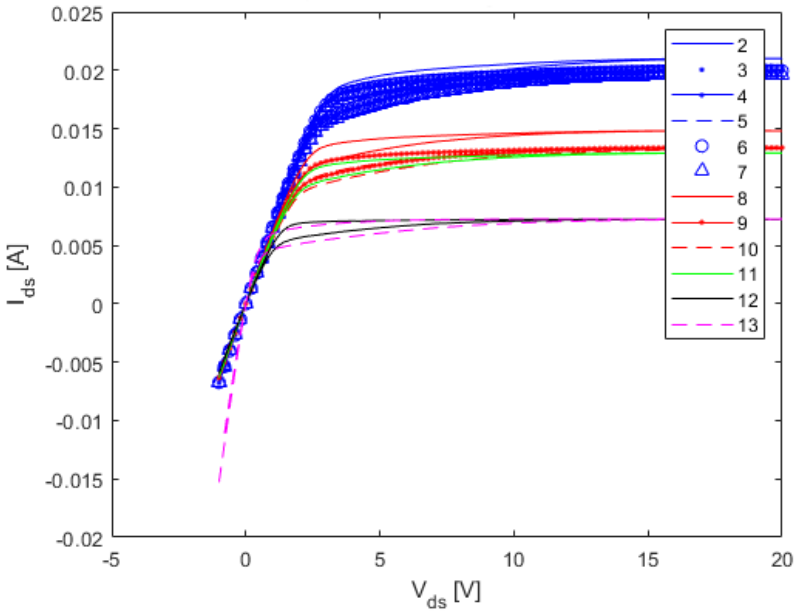

Figure 41. Output curve, i.e. drain current as a function of drain voltage where the gate voltage was a constant -2V. The number labels on the data (2-13), correspond with the steps listed in Section 3.4.1. Line 8 indicates the first horizontal line scan across the bottom gate and line 12 indicates the first horizontal line scan across the top gate.

5.3 Analysis

Ionization damage in the active region of an AlGaN/GaN HEMT was captured in situ due to 47 MeV Ge ion irradiation while under bias in a semi-on state. The active region of an AlGaN/GaN HEMT is the interface between the AlGaN and the GaN material layers. The 47 MeV Ge ions interacted with the interface region and associated depletion region under the gate. According to the SRIM calculations, the Bragg curve stopping location of the 47 MeV Ge ions is well into the SiC substrate, indicating ionization damage is the damage mechanism observed. Drain current degradation is observed when a longer ion dwell time is used during a vertical line scan, as discussed in Section 3.4. The ions have more time to interact with the active region of the device with the longer dwell time allowing the in situ drain current measurement to reflect the ionizations induced in the gate region. Saturation of the threshold voltage shift was reached after the first horizontal scan with 47 MeV Ge ions. Interestingly, in Figures 37 and 38, at approximately time = 50 s, there appears to be a plateau in the drain current. This could be related to saturation of the threshold voltage shift caused by the vertical scans that were previously accomplished. The gate current gets more negative, meaning the leakage current going out the gate is increased due to the additional electron/hole pairs caused by the radiation. Because the gate is held at -2V during this irradiation, any positive charge is attracted towards the gate. The drain current decreases during every irradiation of the gate because the impact ionization adds more current. However, the gate current degradation and threshold voltage shift only occur when the irradiation impacts a location the first time. This indicates that a saturation of the threshold voltage shift was determined, similar to an effect observed in MOSFETs [40].

Electrical stress and irradiation studies have linked threshold voltage shifts and decreased transconductance to acceptor and donor traps formed in the GaN and AlGaN

region [11]. In addition to traps, stress/strain changes between the AlGaN and GaN have been shown to cause threshold voltage shifts as well [41]. The magnitude of the threshold voltage shift is dependent on the drain bias during measurement. For example, when V_d=0.1V, ΔV_{th}=0.1V. However, when the V_d=5V during measurement, the ΔV_{th}=0.3V. The traps associated with ionization damage are most likely interface traps between the AlGaN and GaN caused by ionization damage in the semi-on bias state. Patrick, et al, accomplished proton irradiation modeling using a finite-element solver which found that mobility reduction and contact resistance were not enough to account for the changes to threshold voltage, rather, a negatively charged trap density in the AlGaN and GaN layers were needed. Further investigation localized the trap concentration to within 30 nm of the GaN surface [18]. These conditions cause the gate current to degrade due to the creation of traps or stress/strain which affect the number density of electrons within the 2DEG. In situ measurement of gate and drain current during irradiation when compared to pre and post irradiation output curves showed that no additional change to threshold voltage shift was apparent, the fluence of ions established the saturation threshold voltage for this failure mechanism.

Previous research [42] indicated that no threshold voltage shift was observed when 1.7 MeV Ge ions irradiated the gate-drain gap of the same AlGaN/GaN HEMT device, indicating that threshold voltage is only affected when radiation interacts in the active region under the gate. This technique can be used to help inform radiation induced failure mechanisms and may inform reliability standards, though it is uncertain that a direct correlation can be concluded at this time. This research provides an in situ measurement capturing gate current degradation which correlates to threshold voltage shifts likely associated with traps formed in the AlGaN or GaN layer under the gate by 47 MeV Ge ion irradiation in a semi-on bias state.

5.4 Conclusion

The two gates of a 2×50 μm AlGaN/GaN HEMT were identified using a vertical line scan methodology; the drain current degradation measured in situ caused by the ionization damage was used to locate the active region of the device. The center of the first gate was then targeted with ions across the width of the channel in a horizontal line scan and in situ effects to the gate and drain currents were observed. Positive threshold voltage shifts are likely caused by creation of negative traps in the GaN buffer. Measurement of the same devices after a 30-day room temperature annealing indicated that the devices did not recover and therefore, were permanently damaged. Transconductance and gate current degradation was likely caused by the creation of acceptor traps from the ionization damage. Since the germanium ions went through the gate, depositing well into the substrate, the decreased drain current was likely caused by trapped charge which decreases mobility from carrier-defect scattering and was not caused by displacement damage effects. A direct correlation of this experiment to an electrical stress experiment is not achievable based solely on these results. However, threshold voltage shifts have been observed in stress experiments, however, as electrical stress is continued, threshold voltage shifts tend to worsen and in some cases recover depending on the material and defect created or filled.

Irradiating different areas of the device using a microbeam allows isolation of performance characteristics that can be directly related to spatially refined radiation interaction phenomena. While in a semi-on state during irradiation with 47 MeV Ge ions, irradiating the source produced no change to drain or gate current output. Irradiating the drain produced a photo-current response to drain current output and no change to gate current output. Irradiating the gate produced drain and gate current degradation in an initial irradiation followed by only drain current degradation

in subsequent irradiations. The only situation where post-irradiation characteristic measurements were affected was when the gate was irradiated.

VI. Summary and Future Work

6.1 Summary of Findings

Microscale beams of germanium ions were used to target different locations of AlGaN/GaN HEMTs to determine location dependent radiation effects. The gap between the gate and the drain was targeted with 1.7 MeV Ge ions to observe displacement damage effects. The gate was targeted with 47 MeV Ge ions to observe ionization damage effects. Electrical data was taken pre, during, and post irradiation. To separate transient from permanent degradation, the devices were characterized after a room temperature anneal of at least 30 days. Optical images were also analyzed pre and post irradiation when necessary. This is the first use of localized dynamic irradiation testing has been used to compare AlGaN/GaN HEMT performance ot the results of stress testing via in situ measurements of the gate and drain currents.

Ten AlGaN/GaN HEMTs were irradiated with 1.7 MeV germanium ions using the Micro-ONE system enabling targeting of the gate-drain gap of the HEMTs. In situ measurements captured degradation in the on and semi-on bias conditions after varying levels of ion fluence; no change in the off bias condition during in situ measurement was observed. Pre and post-irradiation output and transfer performance characteristics were compared and analyzed. Changes to the performance characteristics in the on, off and semi-on bias conditions were observed including decreased transconductance, decreased drain current and changes to the Schottky gate-diode forward characteristics, but with no change to the threshold voltage. An offset between the start of the ion irradiation and an increased degradation in gate current was observed for both the on and semi-on state bias. An offset between the start of ion irradiation and a decrease in drain current was also observed for the semi-on bias state. Immediate degradation to the drain current at the start of the ion irradiation

was observed in the on bias state. These observed changes to AlGaN/GaN HEMT device characteristics during 1.7 MeV Ge ion irradiation are correlated to similar performance degradation mechanisms observed in previous HEMT reliability studies such as the inverse piezoelectric effect.

Multiple AlGaN/GaN HEMTs were irradiated by targeting 47 MeV Ge ions through the gate active region while the device was held in a semi-on bias state using the Micro-ONE system. The ionization damage reduced the drain current when the ions interacted with the gate active region during in situ measurements. To exploit this phenomenon, a vertical line scan was accomplished in a top-down and bottom-up fashion across the two gate, common drain device also used in the gate-drain gap experiment. The two scans were compared and the ion beam was centered, using the drain current degradation to determine the center point of both the active gate regions on the dual-gated device. The device was then irradiated using a single horizontal ion line scan targeting the center of one gate in a semi-on state while measuring the drain and gate currents in situ; pre and post irradiation characteristics were compared and analyzed. The technique of targeting the gate using opposing vertical line scans and then irradiating the gate in a semi-on state was repeated on all three devices.

In situ measurements during the 47 MeV Ge ion irradiation of the gate region resulted in drain and gate current degradation which corresponded to a positive threshold voltage shift and reductions in the transconductance and drain current during post irradiation measurements. When a second horizontal ion line scan was conducted, only drain current degradation was observed during in situ measurements, which did not correspond to an additional threshold voltage shift. There was a slight transconductance reduction at higher gate voltages and a decrease in drain current during post-irradiation measurements. Therefore, the threshold voltage shift saturated after the initial line scan. The devices were characterized after a 30 day room temperature

anneal which did not show additional change to threshold voltage indicating the damage to the devices was permanent. This suggests that the gate current degradation is caused by traps formed under the gate and is associated with a threshold voltage shift.

These experiments show that in situ drain and gate current degradation can be captured by using a narrow targeted ion beam, such as the Micro-ONE system at Sandia National Laboratories. This information can be correlated to degradation in performance characterization and can also determine location specific fluence limits. By varying bias states during irradiation, information regarding combined irradiation and bias susceptibility is also captured in situ by observing the drain and gate current responses. Qualification protocols for radiation and intrinsic reliability can be improved by using this technique to understand failure limits due to defects and radiation damage. This information can be used to inform both the reliability and radiation-hardness communities and to help establish testing protocols, develop tolerance limits, and improve physics of failure models.

6.2 Future Work

6.2.1 Further Analysis of this Work

A complete analysis of the Ge ions interacting with the different layers of the AlGaN/GaN HEMT devices should be accomplished to determine the likely traps that were created in both experiments presented in this research. Determining the possible trap energies through modeling and simulation with known trap energies caused by radiation and stress failure mechanisms would enable resolution of the defect or defects that cause the degradation observed in this research. Next, physics-based device modeling and simulation should be accomplished to validate the results and provide more context to the experiments presented in this research. Additional

physics-based modeling could be used to determine which failure mechanisms are forming within the device as a function of time as ions interact at a specific location and to replicate the in situ measurements of the gate and drain current degradation under bias as observed in this research.

6.2.2 Correlation between Radiation and Stress-Testing Defects

This research irradiated the majority of the devices to failure, therefore, finding the initial failure mechanisms was not possible. This research set out to determine if targeting ions at a specific region of a device would provide usable information. To cause maximum damage in that region by either displacement damage or ionization damage was the objective. Using the ion beam to aggravate a known defect in an AlGaN/GaN HEMT caused by a particular reliability stress condition would be extremely useful to the reliability community. Unfortunately, defects caused by reliability stress testing are still an area of active research and not completely understood. Therefore, using the trap energies found from the Ge ion damage and determining if a reliability test can be designed to create a similar defects as the irradiation might be useful as a starting point to further understand the correlation. If the test developed is considered useful, then targeted ion radiation could be used as a tool for replicating reliability test predictions in less time than the 1000 hour stress tests currently in use today. If additional targeted experiments are designed to a non-critical fluence, then pre and post failure mechanism analysis can be accomplished using additional resources beyond current-voltage data.

6.2.3 Scan Across the Gate with a Narrower Ion Beam

An additional area of future research is to scan across the gate width. This is a set-up similar to the vertical scan used in the 47 MeV Ge ion gate experiment. This

may allow the change in the rate of degradation as the beam moves across the gate width and beyond the gate into the gate-drain gap to be measured. Unfortunately, the ion beam full-width half max is of the same order of magnitude as the gate width. A narrower beam is required to perform an in situ measurement of the rate of degradation across this region.

6.2.4 Long Term Reliability Predictions

Understanding how long term reliability is affected by radiation is an area of active research. Therefore, determining if long-term reliability degradation can be calculated and/or predicted with the help of the ion microbeam could be a follow-on project. For example, the ion beam could target specific areas of devices and they could then be stressed to determine the long term reliability of each device. This would help determine whether the long term reliability changes depend on the region of the device irradiated. Applying a bias during irradiation and then accomplishing the long term reliability stress testing calculations could also inform predictions of device performance. Post-irradiation measurement testing or subsequent measurements after room temperature or high temperature annealing can be used to better understand the implications of irradiation of a specific device location, which can ultimately inform the qualification protocol for AlGaN/GaN HEMT devices.

6.2.5 Correlating Ge Ion Damage to Neutron Damage

Since germanium is one of the stable products formed after neutron absorption by gallium, correlating neutron irradiation induced degradation to the degradation observed in this research would be interesting. In particular, targeting the gate-drain gap experiment with neutrons in a similar manner to the experiment conducted in this research where Ge ions were implanted in the interface region where the 2DEG is

formed, would be a good experiment to determine the effects of neutron absorption. Additionally, neutrons cause displacement damage as seen with the 1.7 MeV Ge ions. A correlation between location based ion damage and neutron damage could be made thus providing valuable information to the radiation community.

Bibliography

[1] B.D. Christiansen, R.A. Coutu, E.R. Heller, B.S. Poling, G.D. Via, R. Vetury, and J.B. Shealy. "Reliability Testing of AlGaN/GaN HEMTs under Multiple Stressors." *IRPS 11-681. IEEE International*. CD.2.1-2.5. 2011.

[2] B.D. Christiansen. "Investigation of gallium nitride transistor reliability through accelerated life testing and modeling." Dissertation. AFIT. 2011.

[3] J. Scarpula and C. Gee. "Space Qualification of GaN HEMTs - Guidance Document Announcement." *NASA NEPP*. The Aerospace Corporation. 2018.

[4] S.J. Pearton, F. Ren, E. Patrick, M.E. Law and A. Y. Polyakov. "Review-Ionizing Radiation Damage Effects on GaN Devices." *ECS Journal of Solid State Science and Technology*. 5(2) Q35-Q60 2016.

[5] J. Chen, Y.S. Puzyrev, R. Jiang, E.X. Zhang, M.W. McCurdy, D.M. Fleetwood, R.D. Schrimpf, S.T. Pantelides, A.R. Arehart, S.A. Ringel, P. Saunier and C. Lee. "Effects of Applied Bias and High Field Stress on Radiation Response of GaN/AlGaN HEMTs." *IEEE Transactions on Nuclear Science*. 62(6), 2423-2430. 2015.

[6] J. Chen. "Radiation Response and Reliability of High Speed AlGaN/GaN HEMTS." Dissertation. Vanderbilt University. August, 2016.

[7] B.S. Poling, G.D. Via, K.D. Bol, E.E. Johnson and J.M McDermott. "Commercial-off-the-shelf AlGaN/GaN HEMT device reliability study after exposure to heavy ion radiation." *Microelectronics Reliability.*, 68:13-20, 2017.

[8] Government of the United States as Represented by the Secretary of the Air Force. "Proton Radiation as a Tool for Selective Degradation and Physics Based Device Model Test and Calibration." USPTO Patent Applications. 20180308771. October 25, 2018.

[9] S. Dimitrijev."Understanding Semiconductor Devices." Oxford University Press, Inc. 2000.

[10] B.D. Christiansen, E.R. Heller, R.A. Coutu Jr, R. Vetury and J.B. Shealy. "A Very Robust AlGaN/GaN HEMT Technology to High Forward Gate Bias and Current." *Active and Passive Electronic Components*. 1-4. 2012.

[11] R. Jiang, X. Shen, J. Fang, P. Wang, E.X. Zhang, J. Chen, D.M. Fleetwood, R.D. Schrimpf, S.W. Kaun, E.C. Kyle, J.S. Speck and S.T. Pantelides. "Multiple Defects Cause Degradation After High Field Stress in AlGaN/GaN HEMTs." *IEEE Transactions on Device Materials Reliability* 18(3), 364-376. 2018

[12] E. Heller, S. Choi, D. Dorsey, R. Vetury and S. Graham. "Electrical and structural dependence of operating temperature of AlGaN/GaN HEMTs". *Microelectronics Reliability*, 53(6). 872-877. 2013.

[13] Steve Tetlak. TEM imaging of AlGaN/GAN devices. AFRL. Unpublished. 2011.

[14] E. Heller. "A Survey of Observed GaN HEMT Degradation Mechanisms". *MRQW Conference Presentation*. 7-8 February 2017.

[15] E. Heller, et al. "Tools for Test and Evaluation of Emerging Nanoelectronics." AFOSR T and E Portfolio Review. 6-10 Mar 2017.

[16] Y. Hao, J. Zhang, and J. Zang. "Nitride wide bandgap semiconductor material and electronic devices". CRC Press Taylor and Francic Group, Boca Raton, 2016.

[17] O. Ambacher. J. Smart, J.R. Shealy, N.G. Weimann, K. Chu, M. Murphy, W. J. Schaff, L. F. Eastman, R. Dimitrov, L. Wittmer, M. Stutzman, W. Rieger, and J. Hilsenbeck. "Two-dimensional electron gases induced by spontaneous and piezoelectric polarization charges in N- and Ga-face AlGaN/GaN heterostructures." *Journal of Applied Physics*. 85. 3222. 1999.

[18] E.Patrick, M. Law, L. Liu, C.C. Cuervo, Y. Xi, F. Ren and S.J. Pearton. IEEE Trans. Nuc. Sci. 60(6) 2013.

[19] B.M. Paine, S.R. Polmanter, V.T. Ng. N.T. Kubota and C.R. Igancio. "Lifetesting GaN HEMTs with Multiple Degradation Mechanisms." *IEEE Transactions on Device and Materials Reliability*. 15(4):486-494, Dec 2015.

[20] B.M. Paine. "Scaling DC lifetests on GaN HEMT to RF conditions." *Microelectronics Reliability* 55(2015) 2499-2504

[21] E. Zanoni. "GaN HEMT reliability research - a white paper." University of Padova. Department of Information Engineering. Padova. Aug 31, 2017.

[22] D.J. Cheney, E.A. Douglas, L. Liu, C-F Lo, B.P. Gila, F. Ren and S.J. Pearton. "Degradation Mechanism for GaN and GaAs High Speed Transistors." *Materials*. 5(12) 2498-2520. 2012.

[23] E. Zanoni, M. Meneghini, A. Chini, D. Marcon, and G. Meneghesso. "AlGaN/GaN-Based HEMTs Failure Physics and Reliability: Mechanisms affecting the Gate Edge and Schottky Junction." *IEEE Trans. Electron Devices*. 60(10) 3119-3131. 2013.

[24] A. Ionascut-Nedelcescu, C. Carlone, A. Houdayer, H. J. von Bardeleben, J. Cantin and S. Raymond. "Radiation Hardness of Gallium Nitride." *IEEE Transactions on Nuclear Science*. 49(6). 2733-2738. 2002.

[25] A. Johnston. "Reliability and Radiation Effects in Compound Semiconductors." World Scientific Publishing Co. Pte. Ltd. 2010.

[26] G.F. Knoll. "Radiation Detection and Measurement." 4th ed. John Wiley & Sons, Inc. 2010.

[27] B.D. Weaver, P.A. Martin, J.B. Boos, and C.D. Cress. "Displacement Damage Effects in AlGaN/GaN High Electron Mobility Transistors". *IEEE Transactions on Nuclear Science* 59(6). 3077-3080. 2012.

[28] S. Onoda, T. Ohshima, S.I. Sato, K. Yajima, H. Sasaki, Y. Nabeshima and A. Hasuike. "Enhanced Charge Collection by Single Ion Strike in AlGaN/GaN HEMTs." *IEEE Transactions on Nuclear Science*. 60(6). 4446-4450. 2013.

[29] S. Kuboyama, A. Maru, H. Shindou, N. Ikeda, T. Hirao, H. Abe, and T. Tamura. "Single-Event Damages Caused by Heavy Ions Observed in AlGaN/GaN HEMTs" *IEEE Transactions on Nuclear Science*. 58(6). 2734-2738. 2011.

[30] J. Luo, R. Liu and L. Jiang. "Cross section measurements for gallium in the neutron energy range of 13.5 to 14.8 MeV." *Radiochimica Acta* 100(4). 231-235. 2012.

[31] G.S. Was, Z. Jiao, E. Getto, K. Sun, A.M. Monterrosa, S.A. Maloy, O. Anderoglu, B.H. Sencer, and M. Hackett. "Emulation of reactor irradiation damage using ion beams." *Scripta Materialia*. 88. 33-36. 2014.

[32] M. Rahman, A. Al-Ajili, R. Bates, A. Blue, W. Cunningham, F. Doherty, M. Glaser, L. Haddad, M. Horn, J. Melone, M. Mikuz, T. Quinn, P. Roy, V. O'Shea, K. M. Smith, J. Vaitkus, and V. Wright. *IEEE Transactions on Nuclear Science*. 51(5). 2256-2261. 2004.

[33] J.F. Ziegler, J.P. Biersack, M.D. Ziegler. "SRIM The Stopping and Range or Ions in Matter." www.srim.org. 2013.

[34] D.J. Cheney. "Determination of Semiconductor Device Reliability through electrical and optical characterization and stressing." Dissertation. University of Florida. 2012.

[35] E. Zanoni, G. Meneghesso, G. Verzellesi, F. Danesin, M. Meneghini, F. Rampazzo, A. Tazzoli, and F. Zanon. "A review of failure modes and mechanisms of GaN-based HEMTs." *2007 IEEE International Electron Devices Meeting*. 381-384. 2007.

[36] J.A. del Alamo and J. Joh. "GaN HEMT Reliability." *Microelectronics Reliability* 49(9). 1200-1206. 2009.

[37] J. Joh. and J.A. del Alamo "Critical Voltage for Electrical Degradation of GaN High-Electron Mobility Transistors" *IEEE Electron Device Letters* 29(4). 287-289. 2008.

[38] C.H. Chen, R. Sadler, D. Wang, D. Hou, Y. Yang, W. Yau, W. Sutton, J.C. Shim, S. Wang and A. Duong. "The causes of GaN HEMT bell-shaped transconductance degradation." *Solid-State Electronics.* 126. 115-124. 2016.

[39] G. Vizkelethy. Unpublished Report. February 25-Mar 1. 2019.

[40] H.E. Boesch, F.B. McLean, J.M. Benedetto, J.M. McGarrity and W.E. Bailey. "Saturation of Threshold Voltage Shift in MOSFET's at High Total Dose." *IEEE Transactions on Nuclear Science.* 33(6). 1191-1197. 1986.

[41] A.F. Wilson, A. Wakejima and T.Egawa. "Influence of GaN Stress on Threshold Voltage Shift in AlGaN/GaN High-Electron-Mobility Transistors on Si under Off-state Electrical Bias." *Applied Physics Express* 6(8). 2013.

[42] M. Mace, J. McClory, J. Petrosky and G. Vizkelethy. "Targeted Heavy-Ion Radiation of AlGaN/GaN HEMT." *HEART Conference Proceedings.* 2019.

Vita

Major Melanie Mace graduated from North Mason High School in Belfair, Washington in 2000. She attended Embry-Riddle Aeronautical University in Daytona Beach, Florida where she studied Engineering Physics with a minor in Mathematics. She commissioned in 2005 upon degree completion through the Air Force Reserve Officer Training Corps.

Melanie was assigned the 61D career field, Physics/Nuclear Engineer, however was given the opportunity to completed an operational experience tour in the 13N career field (Missiles). Her first operational assignment was with the 320th Missile Squadron at F.E. Warren AFB, Wyoming as an ICBM launch officer. While at F.E. Warren she completed over 150 alerts as an ICBM Crew Commander, Instructor, and Alternate Command Post (ACP) Commander. As the ACP Commander, she was responsible for 150 on-alert ICBMs and over 100 alert officers and staff. Her final position at F.E. Warren was Requirements Section Chief.

In 2010, she was accepted to the Air Force Institute of Technology at Wright Patterson AFB, in Dayton, Ohio where she studied Nuclear Engineering, specializing in neutron detection. Upon graduation with a Masters Degree in 2012 she was selected to work for Major Command Headquarters Air Force Global Strike Command (AFGSC) as Chief, Nuclear Engineering Analysis in the ICBM Operations Division (A3I) at Barksdale AFB, LA. Her position calculated and consolidated the planning factors (accuracy & reliability), fratricide and survivability data of the ICBM Weapon System for delivery to the AFGSC Commander and ultimately was implemented in the USSTRATCOM targeting software. She was hand selected by the AFGSC CV to work on the Force Improvement Program which then became the Continuous Process Improvement/Lessons Learned section of AFGSC A9 during her last year at AFGSC.

Melanie is a lifetime member of Sigma Pi Sigma and Tau Beta Pi. She is a student member of the American Nuclear Society. Additionally, she has a Masters Degree in Tourism Administration with a focus in Event and Meeting Management and Sustainable Destination Management from George Washington University and a Certificate of Completion in the Space Studies Program from the Naval Postgraduate School.

Next, Melanie will head to Virginia to work with the Defense Threat Reduction Agency where she will continue in the nuclear field.

REPORT DOCUMENTATION PAGE

Form Approved
OMB No. 0704-0188

1. REPORT DATE *(DD-MM-YYYY)*	2. REPORT TYPE	3. DATES COVERED *(From - To)*
12-09-2019	Ph.D. Dissertation	Oct 2016-Sep 2019

4. TITLE AND SUBTITLE
Targeted Germanium Ion Irradiation of Aluminum Gallium Nitride /Gallium Nitride High Electron Mobility Transistors

5a. CONTRACT NUMBER

5b. GRANT NUMBER

5c. PROGRAM ELEMENT NUMBER

6. AUTHOR(S)
Mace, Melanie E., Major, USAF

5d. PROJECT NUMBER

5e. TASK NUMBER

5f. WORK UNIT NUMBER

7. PERFORMING ORGANIZATION NAME(S) AND ADDRESS(ES)
Air Force Institute of Technology
Graduate School of Engineering and Management (AFIT/EN)
2950 Hobson Way, Building 640
Wright-Patterson AFB, OH 45433-7765

8. PERFORMING ORGANIZATION REPORT NUMBER
AFIT-ENP-DS-19-S-025

9. SPONSORING / MONITORING AGENCY NAME(S) AND ADDRESS(ES)
POC: Lt Col Robert Heyward (robert.heyward@nnsa.doe.gov)
National Nuclear Security Administration
NNSA NA-22
1000 Independence Ave., S.W.
Washington D.C., 20585

10. SPONSOR/MONITOR'S ACRONYM(S)
NNSA

11. SPONSOR/MONITOR'S REPORT NUMBER(S)

12. DISTRIBUTION / AVAILABILITY STATEMENT
Distribution Statement A. Approved for Public Release; Distribution Unlimited

13. SUPPLEMENTARY NOTES
This material is declared a work of the U.S. Government and is not subject to copyright protection in the United States.

14. ABSTRACT Microscale beams of germanium ions were used to target different locations of aluminum gallium nitride/gallium nitride (AlGaN/GaN) high electron mobility transistors (HEMTs) to determine location dependent radiation effects. 1.7 MeV Ge ions were targeted at the gap between the gate and the drain to observe displacement damage effects while 47 MeV Ge ions were targeted at the gate to observe ionization damage effects. Electrical data was taken pre, during, and post irradiation. To separate transient from permanent degradation, the devices were characterized after a room temperature anneal for at least 30 days. Optical images were also analyzed pre and post irradiation. This is the first time localized dynamic irradiation testing has been used to compare AlGaN/GaN HEMT performance to the results of stress testing via in situ measurements of the gate and drain currents. The 6 MV Tandem Accelerator at Sandia National Laboratories using the Micro-ONE system was used to induce displacement and ionization damage. Displacement damage was caused by 1.7 MeV Ge ions targeting the gate-drain gap of ten HEMTs in the off, on, and semi-on bias states where a fluence dependent delayed response between ion deposition and gate current degradation in the semi-on and on bias state was observed. The delayed response was also observed in the drain current degradation when biased in the semi-on state, while occurring immediately in the on state. Ionization damage was induced by 47 MeV Ge ions targeting the gate region in the semi-on bias state where gate current degradation occurred during the initial irradiation of the gate active region. Drain current degradation occurred in both the initial and subsequent irradiations. Pre and post irradiation output and transfer performance characteristics indicate drain current and transconductance degradation for both experiments in all bias states. No threshold voltage shift was observed during the displacement damage experiment with 1.7 MeV Ge ions. During the ionization experiment, the threshold voltage increased after the initial irradiation with 2×10^{10} cm^{-2} 47 MeV Ge ions across the length of the gate. Subsequent irradiation over the same location and after a 60 day room temperature anneal did not change this threshold voltage shift and the decrease in the drain current and transconductance persisted, indicating permanent damage. The same performance characteristics changes have been associated with reliability stress testing causing similar effective damage in both the gate-drain gap and the gate regions. The observed degradation in device characteristics are consistent with the inverse piezoelectric effect in the displacement damage experiment and charge trapping in the gate region in the ionization experiment. These results show that radiation induced degradation can be captured by using a targeted ion beam in order to determine location dependent fluence limits, thereby informing both reliability and radiation hardness models.

15. SUBJECT TERMS
AlGaN/GaN HEMT, reliability, radiation, heavy-ion, germanium, threshold voltage shift

16. SECURITY CLASSIFICATION OF:			17. LIMITATION OF ABSTRACT	18. NUMBER OF PAGES	19a. NAME OF RESPONSIBLE PERSON
a. REPORT	b. ABSTRACT	c. THIS PAGE			Dr. John W. McClory
U	U	U	UU	118	19b. TELEPHONE NUMBER *(include area code)* (937) 255-6565 x7308

Standard Form 298 (Rev. 8-98)
Prescribed by ANSI Std. Z39.18